
ESTIMATING KNOTS IN BILINEAR SPLINE GROWTH MODELS WITH TIME-INVARIANT COVARIATES IN THE FRAMEWORK OF INDIVIDUAL MEASUREMENT OCCASIONS

A PREPRINT

Jin Liu
Department of Biostatistics
Virginia Commonwealth University
Veronica.Liu0206@gmail.com

Le Kang
Department of Biostatistics
Virginia Commonwealth University

Robert M. Kirkpatrick
Department of Psychiatry
Virginia Commonwealth University

Roy T. Sabo
Department of Biostatistics
Virginia Commonwealth University

Robert A. Perera*
Department of Biostatistics
Virginia Commonwealth University

November 18, 2021

ABSTRACT

The linear spline growth model (LSGM) is a popular tool for examining nonlinear change patterns over time. It approximates complex patterns by attaching at least two linear trajectories. Besides examining within-person changes and between-person differences of trajectories simultaneously, it poses interesting statistical challenges, such as estimating the location of a change point (or knot), the knot's variance, prediction of the knot location using covariates, and analyzing data with individually-varying times points (ITPs). We developed a pair of bilinear spline growth models with time-invariant covariates (BLSGMs-TICs) to estimate a knot and its variability as well as to investigate predictors of individual trajectories in the ITPs framework. Our simulation studies demonstrate that the proposed models are capable of estimating and testing the knot variance while controlling Type I error rates. More importantly, they generally estimate the parameters of interest unbiasedly, precisely and exhibit appropriate confidence interval coverage.

Keywords Linear spline growth models · Unknown knots · Individually-varying time points · Time-invariant covariates · Simulation studies

1 Introduction

Longitudinal studies of change are popular in various disciplines to evaluate individual growth over time. If a process under investigation is followed for a long enough time duration, it is likely to exhibit some degree of nonlinear change in which the curve has a nonconstant relationship to recorded time. Nonlinear change patterns exist in multiple areas, for example, verbal ability (Jones and Bayley, 1941), math ability (Harring, 2009), cognitive accelerated aging (Finkel et al., 2003), and rehabilitation after the total knee arthroplasty (Riddle et al., 2015; Dumenci et al., 2019). When analyzing such trajectories, it is of interest to investigate within-individual change and between-individual differences simultaneously. One approach to examining the mean change pattern and the individual variability around it is the linear spline growth model (LSGM) (Grimm et al., 2016), also referred to as a piecewise linear latent growth model (Sterba, 2014). By allowing for piecewise linear change patterns for distinct periods, it can approximate more complex underlying functional forms. The LSGM can be modeled either in the structural equation modeling (SEM) framework or using a mixed-effects modeling (Grimm et al., 2016). This article focuses on the LSGM in the SEM framework.

*CONTACT Robert A. Perera. Email: robert.perera@vcuhealth.org

Under assumptions that between-subject differences in growth factors (i.e., individuals' intercepts and slopes) follow a multivariate normal distribution and that all individuals belong to one single population (Bollen and Curran, 2005), researchers employed the LSGM to investigate a nonlinear change of an individual over time as well as difference across such individuals' changes through estimating the mean vector and the variance-covariance matrix of such growth factors. When estimating, the LSGM poses several interesting statistical challenges. First of all, besides growth factors such as intercepts and slopes, it is of interest to examine the characteristics of the inflection point or 'knot' at which two segments join together. When fitting LSGMs, knots can be either pre-specified by a theory-driven method (Flora, 2008) or estimated by a data-driven approach (Kwok et al., 2010). A LSGM with a known fixed knot can be fit by specifying a nonlinear function of time t as factor loadings of the slopes (Flora, 2008). For example, researchers employed a multiple-group bilinear spline growth model (BLSGM) with a pre-specified fixed knot to investigate the short- and long-term post-surgical rehabilitation after the surgery of knee replacement and to examine the differences in trajectories across groups (Riddle et al., 2015).

Alternatively, a knot can be viewed as a parameter in a more flexible setting. Harring, Cudeck, and du Toit developed a BLSGM with an unknown fixed knot with a unified functional form of two linear pieces through reparameterization (Harring et al., 2006). More importantly, previous studies provided the transformed matrices for the reparameterized mean vector and variance-covariance matrix of growth factors to allow them to change back to be interpretable after estimation (Kohli, 2011; Kohli et al., 2013; Grimm et al., 2016). By implementing this model, Kohli, Harring, and Hancock examined the development in each stage, and estimated a fixed knot for procedural learning task research (Kohli et al., 2013). In addition, Preacher and Hancock extended the model with an unknown fixed knot to estimate the variance of the inflection point simultaneously, in which the knot was viewed as an extra growth factor besides the intercept and two slopes (Preacher and Hancock, 2015).

Although such developed reparameterized BLSGMs with an unknown knot make it possible to estimate the inflection point as well as its variance conveniently, they may be less useful when being employed to analyze the piecewise change patterns. Firstly, the first growth factor is expressed as the average intercept (Harring et al., 2006), suggesting that the intercept of each linear piece needs to be involved, which is redundant since a bilinear change pattern only requires the initial status, the rate of change of each period, and the knot to demonstrate its entire characteristics.

Secondly, the existing BLSGM to estimate a knot with its variance does not provide transformed and inverse-transformed matrices between the original and the reparameterized growth factors, though such matrices have been presented for the BLSGM with an unknown fixed knot (Kohli, 2011; Kohli et al., 2013; Grimm et al., 2016). The parameters of most interest from such models are the knot and its variance. However, the characteristics of other growth factors, such as the initial status and the rate of the change of each stage, even those of the associations between such growth factors also provide information which helps to capture features of trajectories.

More importantly, to our knowledge, no previous studies concerning the statistical power to detect the between-individual difference of the knot have already been taken, indicating that we are not yet able to decide if we need to consider the variability of the inflection point when fitting the model. Last but not least, the BLSGM with an unknown knot does allow to make inferences for the mean of such nonlinear change patterns for a single group as well as the variability in individual trajectories around the mean change. Still, it is of interest to explore individual-level covariates (also referred to as 'time-invariant covariates') that are associated with the between-individual differences in the trajectories. The current framework does not incorporate subject-level covariates, which prohibits investigation of predictors to explain the variances of the knot and other growth factors.

Another statistical challenge of longitudinal data sets is the individual-varying measurement occasion, which may emerge if time is measured precisely. For example, the measurement is recorded as an exact date instead of months or years. Another possible rationale is a self-initiated response to some specific behaviors. For instance, in an adolescent smoking study, participants were asked to complete a questionnaire on pocket computers immediately after smoking (Hedeker et al., 2006). One possible way to fit the growth model with individual measurement occasions is the definition variable approach, in which the 'definition variables' are defined as observed variables that are employed to adjust model parameters to individual-specific values (Mehta and West, 2000; Mehta and Neale, 2005).

In the SEM framework, demonstrations of how to incorporate the definition variable approach have concerned either linear trajectories (Mehta and West, 2000) or BLSGM with a pre-specified inflection point (Sterba, 2014). However, to our knowledge, no previous studies have demonstrated how to implement BLSGMs with an unknown knot with exactly individually varying measurement time in the SEM framework, although this extension has been recommended (Grimm et al., 2016).

The proposed model fills an existing gap by describing how to fit a BLSGM with time-invariant covariates (BLSGM-TICs) in the individually-varying time points (ITPs) framework to estimate an inflection time point with its variance and other growth factors as well as to explore predictors of between-individual differences in trajectories. To assess

the statistical power of detecting the between-subject difference in the knot, we also develop a BLSGM-TICs for estimating an inflection point without variability. The remainder of this article is organized as follows. In the method section, we first present the model specification of the BLSGM-TICs to estimate an inflection point and its variance. Next, we introduce how to reparameterize growth factors and the corresponding path coefficients from the TICs to the growth factors to make them estimable in the SEM framework and how to transform them back after estimation for interpretation purpose. We then propose one possible reduced BLSGM-TICs to estimate the knot without variance. We finally describe the model estimation as well as the Monte Carlo simulation design for model evaluation. In the result section, we demonstrate the statistical power of detecting the knot variance as well as the evaluation of the model performance concerning the non-convergent rate, the improper solutions, as well as the bias, the root-mean-squared-error (RMSE) and the empirical coverage for a nominal 95% confidence interval of each parameter of interest.

2 Method

2.1 Model Specification

With an assumption that all subjects are from a single population conditional on individual-level covariates, the BLSGM-TICs with an unknown knot is given

$$\mathbf{y}_i = \mathbf{\Lambda}_i(\gamma_i)\boldsymbol{\eta}_i + \boldsymbol{\epsilon}_i, \quad (1)$$

where \mathbf{y}_i is a $J \times 1$ vector of the repeated outcomes for the i^{th} person (in which J is the number of measurements), $\mathbf{\Lambda}_i(\gamma_i)$, which is a function of its unknown knot γ_i , is a $J \times 3$ matrix of factor loadings determined by definition variables, $\boldsymbol{\epsilon}_i$ is a $J \times 1$ vector of residuals for the i^{th} person, and $\boldsymbol{\eta}_i$ is a 3×1 vector of growth factors $\boldsymbol{\eta}_i = (\eta_{0i}, \eta_{1i}, \eta_{2i})^T$, for an intercept and two slopes) of the i^{th} individual. $\boldsymbol{\eta}_i$ can be regressed on individual-level covariates,

$$\boldsymbol{\eta}_i = \boldsymbol{\alpha} + \mathbf{B}\mathbf{X}_i + \boldsymbol{\zeta}_i \quad (2)$$

where $\boldsymbol{\alpha}$ is a 3×1 vector of growth factor intercepts (which is the mean vector of growth factors if the TICs are centered), \mathbf{B} is a $3 \times c$ matrix of regression coefficients (in which c is the number of TICs) from TICs to growth factors, \mathbf{X}_i , which may either be continuous or be categorical, is a $c \times 1$ vector of covariates of the i^{th} individual, and $\boldsymbol{\zeta}_i$ is a 3×1 vector of deviations of the i^{th} subject from the factor means.

Tishler and Zang (Tishler and Zang, 1981; Seber and Wild, 2003) showed that the continuous two-phase regression model can be written as either the minimum or maximum response value of two trajectories. By extending such expressions to the BLSGM framework, two forms of bilinear spline for the i^{th} individual are shown in Figure 1. In the left panel ($\eta_{1i} > \eta_{2i}$), the measurement y_{ij} should always be the minimum value of two lines; that is, $y_{ij} = \min(\eta_{0i} + \eta_{1i}t_{ij}, \eta_{02i} + \eta_{2i}t_{ij})$. To unify the expression of measurements pre- and post-knot, we have the following equation

$$\begin{aligned} y_{ij} &= \min(\eta_{0i} + \eta_{1i}t_{ij}, \eta_{02i} + \eta_{2i}t_{ij}) \\ &= \frac{1}{2}(\eta_{0i} + \eta_{1i}t_{ij} + \eta_{02i} + \eta_{2i}t_{ij} - |\eta_{0i} + \eta_{1i}t_{ij} - \eta_{02i} - \eta_{2i}t_{ij}|) \\ &= \frac{1}{2}(\eta_{0i} + \eta_{1i}t_{ij} + \eta_{02i} + \eta_{2i}t_{ij}) - \frac{1}{2}(|\eta_{0i} + \eta_{1i}t_{ij} - \eta_{02i} - \eta_{2i}t_{ij}|) \\ &= \frac{1}{2}(\eta_{0i} + \eta_{02i} + \eta_{1i}t_{ij} + \eta_{2i}t_{ij}) - \frac{1}{2}(\eta_{1i} - \eta_{2i})|t_{ij} - \gamma_i| \\ &= \eta'_{0i} + \eta'_{1i}(t_{ij} - \gamma_i) + \eta'_{2i}|t_{ij} - \gamma_i| \\ &= \eta'_{0i} + \eta'_{1i}(t_{ij} - \gamma_i) + \eta'_{2i}\sqrt{(t_{ij} - \gamma_i)^2}, \end{aligned} \quad (3)$$

where η'_{0i} , η'_{1i} and η'_{2i} are the measurement at the knot, the mean of two slopes, and the half difference between two slopes. Through straightforward algebra, the measurement y_{ij} of the bilinear spline in the right panel, in which the measurement y_{ij} should always be the maximum value of two lines, has the identical final form as Equation (3).

In the model shown in Equation (1), the inflection point γ_i , like the intercept and two slopes, varies across individuals and then is viewed as an extra factor. SEM models fail to estimate it directly (Grimm et al., 2016), due to the nonlinear relationship between the repeated outcome and the growth factors. The proposed model can be expressed as a linear combination of all four growth factors through the Taylor series expansion (Browne and du Toit, 1991; Grimm et al., 2016). By this approach (see Supplementary 6.1 for detailed derivation), we obtain the reparameterized growth factors and the corresponding factor loadings for the i^{th} individual, which can be expressed as

$$\boldsymbol{\eta}'_i = \begin{pmatrix} \eta'_{0i} & \eta'_{1i} & \eta'_{2i} & \delta_i \end{pmatrix}^T = \begin{pmatrix} \eta_{0i} + \gamma_i\eta_{1i} & \frac{\eta_{1i} + \eta_{2i}}{2} & \frac{\eta_{2i} - \eta_{1i}}{2} & \gamma_i - \mu_\gamma \end{pmatrix}^T \quad (4)$$

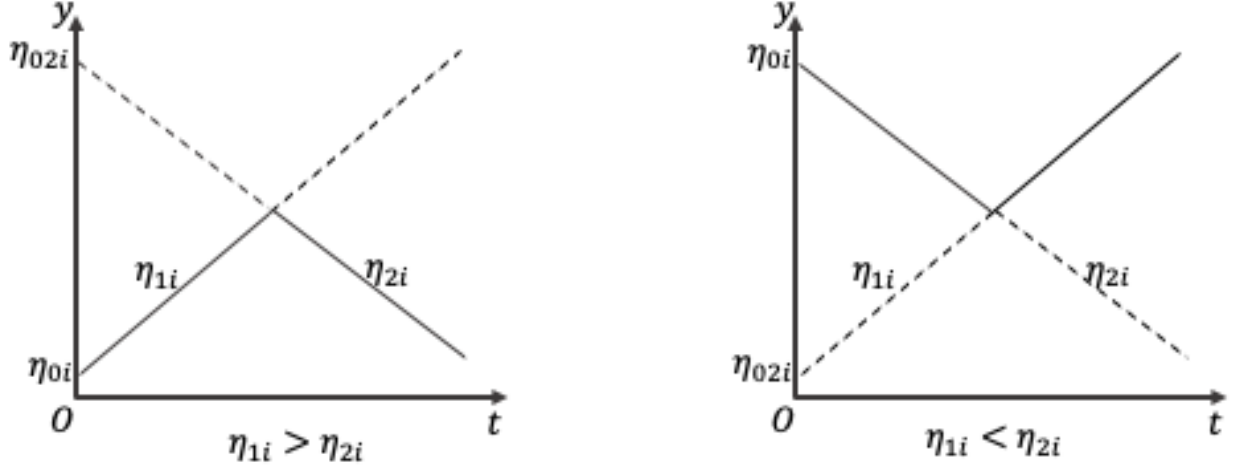


Figure 1: The Two Forms of the Continuous Bilinear Spline

and

$$\Lambda'_i(\gamma_i) = \begin{pmatrix} 1 & t_{ij} - \mu_\gamma & |t_{ij} - \mu_\gamma| & -\mu_{\eta'_2} - \frac{\mu_{\eta'_2}(t_{ij} - \mu_\gamma)}{|t_{ij} - \mu_\gamma|} \end{pmatrix} \quad (j = 1, \dots, J), \quad (5)$$

respectively, where μ_γ is the knot mean and δ_i is the deviation from the knot mean of the i^{th} individual. With η'_i and $\Lambda'_i(\gamma_i)$ as shown in Equations (4) and (5), we then respecify the BLSGM-TICs in Equations (1) and (2) as Equations

$$\mathbf{y}_i = \Lambda'_i(\gamma_i) \eta'_i + \epsilon_i \quad (6)$$

and

$$\eta'_i = \alpha' + B' X_i + \zeta'_i, \quad (7)$$

respectively, where α' is a 4×1 vector of reparameterized growth factor intercepts while B' is a $4 \times c$ matrix of reparameterized path coefficients (in which c is the number of TICs) from TICs to the growth factors, and ζ'_i is a 4×1 vector of normally distributed deviations of the i^{th} individual from the reparameterized growth factor means. Such growth factor intercepts and coefficients also needed to be transformed back to be interpretable as the relationship between the growth factors in the original setting.

2.2 Transformed Matrix and Inverse-transformed Matrix

When fitting a model in the SEM framework, especially a complex model, it is vital to select a proper set of initial values to improve convergence and accelerate the computational process. Generally, descriptive statistics and visualization are tools for researchers to decide suitable initial values for the parameters of interest. However, it may not be straightforward for the reparameterized parameters. Accordingly, the transformed matrices from parameters in the original frame to those in the reparameterized setting are helpful to decide appropriate initial values. More importantly, all reexpressed parameters need to be transformed back to be interpretable after estimating, which can be realized by inverse-transformed matrices. With straightforward algebra, we obtain the transformed and inverse-transformed matrices for the mean vectors and the variance-covariance matrices.

For the i^{th} individual, as shown in Equation (4), the relationships between the original growth factors (η_i) and the reparameterized growth factors (η'_i) are G_i and G_i^{-1} are given by

$$\begin{aligned} \eta'_i &= \begin{pmatrix} \eta'_{0i} & \eta'_{1i} & \eta'_{2i} & \delta_i \end{pmatrix}^T = \begin{pmatrix} \eta_{0i} + \gamma_i \eta_{1i} & \frac{\eta_{1i} + \eta_{2i}}{2} & \frac{\eta_{2i} - \eta_{1i}}{2} & \gamma_i - \mu_\gamma \end{pmatrix}^T \\ &= \begin{pmatrix} 1 & \gamma_i & 0 & 0 \\ 0 & 0.5 & 0.5 & 0 \\ 0 & -0.5 & 0.5 & 0 \\ 0 & 0 & 0 & 1 \end{pmatrix} \begin{pmatrix} \eta_{0i} \\ \eta_{1i} \\ \eta_{2i} \\ \gamma_i - \mu_\gamma \end{pmatrix} = G_i \times \begin{pmatrix} \eta_{0i} \\ \eta_{1i} \\ \eta_{2i} \\ \gamma_i - \mu_\gamma \end{pmatrix} \end{aligned}$$

and

$$\begin{aligned} \boldsymbol{\eta}_i &= (\eta_{0i} \ \eta_{1i} \ \eta_{2i} \ \gamma_i)^T = (\eta'_{0i} - \gamma_i \eta'_{1i} + \gamma_i \eta'_{2i} \ \eta'_{1i} - \eta'_{2i} \ \eta'_{1i} + \eta'_{2i} \ \delta_i + \mu_\gamma)^T \\ &= \begin{pmatrix} 1 & -\gamma_i & \gamma_i & 0 \\ 0 & 1 & -1 & 0 \\ 0 & 1 & 1 & 0 \\ 0 & 0 & 0 & 1 \end{pmatrix} \begin{pmatrix} \eta'_{0i} \\ \eta'_{1i} \\ \eta'_{2i} \\ \delta_i + \mu_\gamma \end{pmatrix} = \mathbf{G}_i^{-1} \times \begin{pmatrix} \eta'_{0i} \\ \eta'_{1i} \\ \eta'_{2i} \\ \delta_i + \mu_\gamma \end{pmatrix}. \end{aligned}$$

It is noted that the (inverse-) transform matrix is individual-level due to the variability of the knot. For implementation, we employ the population-level (inverse-) transform matrix to simplify the calculation. In Supplementary 6.2, we present the conditions under which the individual-level matrices can be approximated to be the population-level ones.

The transformed matrix and the inverse-transformed matrix between the mean vector of the original growth factors ($\boldsymbol{\mu}_\eta$) and that of the reparameterized growth factors ($\boldsymbol{\mu}_{\eta'}$) are

$$\boldsymbol{\mu}_{\eta'} \approx \begin{pmatrix} 1 & \mu_\gamma & 0 & 0 \\ 0 & 0.5 & 0.5 & 0 \\ 0 & -0.5 & 0.5 & 0 \\ 0 & 0 & 0 & 1 \end{pmatrix} \times \begin{pmatrix} \mu_{\eta_0} \\ \mu_{\eta_1} \\ \mu_{\eta_2} \\ 0 \end{pmatrix} = \mathbf{G} \times \begin{pmatrix} \mu_{\eta_0} \\ \mu_{\eta_1} \\ \mu_{\eta_2} \\ 0 \end{pmatrix}$$

and

$$\boldsymbol{\mu}_\eta \approx \begin{pmatrix} 1 & -\mu_\gamma & \mu_\gamma & 0 \\ 0 & 1 & -1 & 0 \\ 0 & 1 & 1 & 0 \\ 0 & 0 & 0 & 1 \end{pmatrix} \times \begin{pmatrix} \mu_{\eta'_0} \\ \mu_{\eta'_1} \\ \mu_{\eta'_2} \\ \mu_\gamma \end{pmatrix} = \mathbf{G}^{-1} \times \begin{pmatrix} \mu_{\eta'_0} \\ \mu_{\eta'_1} \\ \mu_{\eta'_2} \\ \mu_\gamma \end{pmatrix};$$

and those between the variance-covariance matrix of the original growth factors ($\boldsymbol{\Psi}_\eta$) and that of the reparameterized growth factors ($\boldsymbol{\Psi}_{\eta'}$) are

$$\begin{aligned} \boldsymbol{\Psi}_{\eta'} &\approx E(\text{Var}(\mathbf{G}_i \times \boldsymbol{\eta}_i | \gamma_i)) = E(\nabla \mathbf{G}_i \text{Var}(\boldsymbol{\eta}_i) \nabla \mathbf{G}_i^T) \\ &\approx \begin{pmatrix} 1 & \mu_\gamma & 0 & \mu_{\eta_1} \\ 0 & 0.5 & 0.5 & 0 \\ 0 & -0.5 & 0.5 & 0 \\ 0 & 0 & 0 & 1 \end{pmatrix} \boldsymbol{\Psi}_\eta \begin{pmatrix} 1 & \mu_\gamma & 0 & \mu_{\eta_1} \\ 0 & 0.5 & 0.5 & 0 \\ 0 & -0.5 & 0.5 & 0 \\ 0 & 0 & 0 & 1 \end{pmatrix}^T \\ &= \nabla \mathbf{G} \boldsymbol{\Psi}_\eta \nabla \mathbf{G}^T \end{aligned}$$

and

$$\begin{aligned} \boldsymbol{\Psi}_\eta &\approx E(\text{Var}(\mathbf{G}_i^{-1} \times \boldsymbol{\eta}'_i | \gamma_i)) = E(\nabla \mathbf{G}_i^{-1} \text{Var}(\boldsymbol{\eta}'_i) \nabla \mathbf{G}_i^{-1T}) \\ &\approx \begin{pmatrix} 1 & -\mu_\gamma & \mu_\gamma & 0 \\ 0 & 1 & -1 & 0 \\ 0 & 1 & 1 & 0 \\ 0 & 0 & 0 & 1 \end{pmatrix} \boldsymbol{\Psi}_{\eta'} \begin{pmatrix} 1 & -\mu_\gamma & \mu_\gamma & 0 \\ 0 & 1 & -1 & 0 \\ 0 & 1 & 1 & 0 \\ 0 & 0 & 0 & 1 \end{pmatrix}^T \\ &= \nabla \mathbf{G}^{-1} \boldsymbol{\Psi}_{\eta'} \nabla \mathbf{G}^{-1T}. \end{aligned}$$

When fitting the BLSGM-TICs using an *R* package such as *OpenMx*, which allows for matrix calculation, we only need to provide the matrices \mathbf{G} , \mathbf{G}^{-1} , $\nabla \mathbf{G}$ and $\nabla \mathbf{G}^{-1}$ for transformation between the original setting and the reparameterized frame. In contrast, when (inversely) transforming parameters using other SEM software like *Mplus*, we need to give an expression of each cell of the mean vectors and the variance-covariance matrices, all of which are provided in Supplementary 6.3.

When regressing growth factors on the individual-level covariates as we did in Equation (2), we also need to reexpress the path coefficients if we reparameterize the growth factors. By centering the covariates, on the one hand, we make the vector $\boldsymbol{\alpha}$ equivalent to the mean vector of growth factor. Accordingly, the transformed and inverse-transformed matrices between the original intercepts ($\boldsymbol{\alpha}$) and the reparameterized intercepts ($\boldsymbol{\alpha}'$) are \mathbf{G} and \mathbf{G}^{-1} , respectively. On the other hand, through centering the covariates, we simplify the transformed and inverse-transformed matrices between the original path coefficients (\mathbf{B}) and the reparameterized path coefficients (\mathbf{B}') as $\nabla \mathbf{G}$ and $\nabla \mathbf{G}^{-1}$, respectively. The detailed derivation is shown in Supplementary 6.4.

2.3 Model Estimation

To simplify estimation, we assume that the growth factors (the intercept, two slopes and the knot) are normally distributed conditional on individual-level covariates and that individual residuals follow identical and independent normal distributions over time, that is, $\epsilon_i \sim N(0, \theta_\epsilon \mathbf{I})$. Then for the i^{th} individual, the expected mean vector and the variance-covariance structure of the repeated measurements of the model given in Equations (6) and (7) can be expressed as²

$$\boldsymbol{\mu}_i = \boldsymbol{\Lambda}'_i(\gamma_i)(\boldsymbol{\alpha}' + \mathbf{B}' \boldsymbol{\mu}_X) \quad (8)$$

and

$$\boldsymbol{\Sigma}_i = \boldsymbol{\Lambda}'_i(\gamma_i) \boldsymbol{\Psi}_\eta \boldsymbol{\Lambda}'_i(\gamma_i)^T + \boldsymbol{\Lambda}'_i(\gamma_i) \mathbf{B}' \boldsymbol{\Phi} \mathbf{B}'^T \boldsymbol{\Lambda}'_i(\gamma_i)^T + \theta_\epsilon \mathbf{I}, \quad (9)$$

where $\boldsymbol{\mu}_X$ and $\boldsymbol{\Phi}$ are the mean vector ($c \times 1$) and the variance-covariance matrix ($c \times c$) of the TICs, respectively, other parameters have the exactly same definition in Equations (6) and (7).

The parameters in the model given in Equations (6) and (7) include the mean vector and the variance-covariance matrix of reparameterized growth factors, the reexpressed path coefficients as well as the means and the variance-covariance structure of subject-level covariates. Then by the inverse-transformed matrices provided in Section 2.2, the parameters in the original setting can be calculated. $\boldsymbol{\Theta}_1$ and $\boldsymbol{\Theta}'_1$ in Equations

$$\begin{aligned} \boldsymbol{\Theta}_1 &= \{\boldsymbol{\alpha}, \boldsymbol{\Psi}_\eta, \mathbf{B}, \boldsymbol{\mu}_X, \boldsymbol{\Phi}, \theta_\epsilon\} \\ &= \{\mu_{\eta_0}, \mu_{\eta_1}, \mu_{\eta_2}, \mu_\gamma, \psi_{00}, \psi_{01}, \psi_{02}, \psi_{0\gamma}, \psi_{11}, \psi_{12}, \psi_{1\gamma}, \psi_{22}, \psi_{2\gamma}, \psi_{\gamma\gamma}, \mathbf{B}, \boldsymbol{\mu}_X, \boldsymbol{\Phi}, \theta_\epsilon\} \end{aligned} \quad (10)$$

and

$$\begin{aligned} \boldsymbol{\Theta}'_1 &= \{\boldsymbol{\alpha}', \boldsymbol{\Psi}'_\eta, \mathbf{B}', \boldsymbol{\mu}_X, \boldsymbol{\Phi}, \theta_\epsilon\} \\ &= \{\mu'_{\eta_0}, \mu'_{\eta_1}, \mu'_{\eta_2}, \mu_\gamma, \psi'_{00}, \psi'_{01}, \psi'_{02}, \psi'_{0\gamma}, \psi'_{11}, \psi'_{12}, \psi'_{1\gamma}, \psi'_{22}, \psi'_{2\gamma}, \psi_{\gamma\gamma}, \mathbf{B}', \boldsymbol{\mu}_X, \boldsymbol{\Phi}, \theta_\epsilon\} \end{aligned} \quad (11)$$

list the parameters in the original and the reparameterized frames, respectively.

We then use full information maximum likelihood (FIML) to estimate $\boldsymbol{\Theta}'_1$ due to the potential heterogeneity of individual contributions (which are specified by definition variables) to the likelihood. The log-likelihood function of each individual and that of the overall sample can be expressed as

$$\log \text{lik}_i(\boldsymbol{\Theta}'_1 | \mathbf{y}_i) = C - \frac{1}{2} \ln |\boldsymbol{\Sigma}_i| - \frac{1}{2} (\mathbf{y}_i - \boldsymbol{\mu}_i)^T \boldsymbol{\Sigma}_i^{-1} (\mathbf{y}_i - \boldsymbol{\mu}_i), \quad (12)$$

and

$$\log \text{lik}(\boldsymbol{\Theta}'_1 | \mathbf{y}) = \sum_{i=1}^n \log \text{lik}_i(\boldsymbol{\Theta}'_1 | \mathbf{y}_i), \quad (13)$$

respectively (Hoyle, 2012), where C is a constant, n is the number of individuals, $\boldsymbol{\mu}_i$ and $\boldsymbol{\Sigma}_i$ are the mean vector and the variance-covariance matrix of \mathbf{y}_i , which have been defined in Equations (8) and (9), respectively. We construct the proposed BLSGM-TICs using the R package *OpenMx* with the optimizer CSOLNP (Neale et al., 2016; Pritikin et al., 2015; Hunter, 2018; Boker et al., 2018), with which we are able to fit the proposed model and implement the transformed matrix as well as inverse-transformed matrix as shown in Section 2.2 efficiently.

2.4 Reduced Model

By fixing the between-individual differences in the inflection point to 0, the model in Equation (1) has a reduced form for estimating an unknown knot without considering variability given by

$$\mathbf{y}_i = \boldsymbol{\Lambda}_i(\gamma) \boldsymbol{\eta}_i + \boldsymbol{\epsilon}_i, \quad (14)$$

where $\boldsymbol{\Lambda}_i(\gamma)$, which is a function of a fixed inflection point γ , is a $J \times 3$ matrix of factor loadings.

When being modeled in the SEM framework, this reduced model still needs to be reparameterized to be a unified linear combination of growth factors with multiple approaches available to realize it (Harring et al., 2006; Grimm et al., 2016). In this article, we express the repeated measurements of the outcome as we did in Equation (3) and accordingly write the reparameterized growth factors and the corresponding factor loadings as

$$\boldsymbol{\eta}'_i = \begin{pmatrix} \eta'_{0i} & \eta'_{1i} & \eta'_{2i} \end{pmatrix}^T = \begin{pmatrix} \eta_{0i} + \gamma \eta_{1i} & \frac{\eta_{1i} + \eta_{2i}}{2} & \frac{\eta_{2i} - \eta_{1i}}{2} \end{pmatrix}^T \quad (15)$$

²We extend the expressions of the expected mean vector and variance-covariance structure of repeated measurements in a study of Grimm, Ram, and Estabrook (Grimm et al., 2016) to the framework of our model.

and

$$\Lambda'_i(\gamma) = (1 \quad t_{ij} - \gamma \quad |t_{ij} - \gamma|) \quad (j = 1, \dots, J). \quad (16)$$

The transformed and inverse-transformed matrices are also reduced accordingly. Specifically, we only need the first three rows and the first three columns in such matrix functions as \mathbf{G} , \mathbf{G}^{-1} , $\nabla \mathbf{G}$ and $\nabla \mathbf{G}^{-1}$, since only three growth factors need to be reparameterized. It is noted that the population-level (inverse-) transformed matrix is the same as the individual-level (inverse-) transformed matrix for the reduced model.

For the i^{th} individual, the expected mean vector and the variance-covariance matrix of the repeated outcomes of this model are

$$\boldsymbol{\mu}_i = \Lambda'_i(\gamma)(\boldsymbol{\alpha}' + \mathbf{B}' \boldsymbol{\mu}_X) \quad (17)$$

and

$$\boldsymbol{\Sigma}_i = \Lambda'_i(\gamma) \boldsymbol{\Psi}_\eta \Lambda'_i(\gamma)^T + \Lambda'_i(\gamma) \mathbf{B}' \boldsymbol{\Phi} \mathbf{B}'^T \Lambda'_i(\gamma)^T + \theta_\epsilon \mathbf{I}, \quad (18)$$

respectively, in which the dimensions of $\boldsymbol{\alpha}'$ and \mathbf{B}' are 3×1 and $3 \times c$ (i.e., the first three rows of such in Equations (8) and (9)), respectively. For this reduced model, $\boldsymbol{\Theta}_2$ and $\boldsymbol{\Theta}'_2$ are defined as

$$\begin{aligned} \boldsymbol{\Theta}_2 &= \{ \boldsymbol{\alpha}, \gamma, \boldsymbol{\Psi}_\eta, \mathbf{B}, \boldsymbol{\mu}_X, \boldsymbol{\Phi}, \theta_\epsilon \} \\ &= \{ \mu_{\eta_0}, \mu_{\eta_1}, \mu_{\eta_2}, \gamma, \psi_{00}, \psi_{01}, \psi_{02}, \psi_{11}, \psi_{12}, \psi_{22}, \mathbf{B}, \boldsymbol{\mu}_X, \boldsymbol{\Phi}, \theta_\epsilon \} \end{aligned} \quad (19)$$

and

$$\begin{aligned} \boldsymbol{\Theta}'_2 &= \{ \boldsymbol{\alpha}', \gamma, \boldsymbol{\Psi}'_\eta, \mathbf{B}', \boldsymbol{\mu}_X, \boldsymbol{\Phi}, \theta_\epsilon \} \\ &= \{ \mu'_{\eta_0}, \mu'_{\eta_1}, \mu'_{\eta_2}, \gamma, \psi'_{00}, \psi'_{01}, \psi'_{02}, \psi'_{11}, \psi'_{12}, \psi'_{22}, \mathbf{B}', \boldsymbol{\mu}_X, \boldsymbol{\Phi}, \theta_\epsilon \}, \end{aligned} \quad (20)$$

and list the parameters in the original and reparameterized setting, respectively. By replacing $\boldsymbol{\Theta}'_1$ in Equations (12) and (13) with $\boldsymbol{\Theta}'_2$ and updating $\boldsymbol{\mu}_i$ and $\boldsymbol{\Sigma}_i$ as such defined in Equations (17) and (18), we have the likelihood function of each individual and that of the overall sample. We build the reduced model using the R package *OpenMx* with the optimizer CSOLNP and employ the FIML technique to estimate the parameters. We provide the *OpenMx* syntax for the proposed BLSGM-TICs and its reduced version as well as a demonstration in the online appendix (https://github.com/Veronica0206/Dissertation_projects). For the researchers who are willing to use *Mplus*, we also provide *Mplus* 8 syntax for both models in the online appendix.

3 Model Evaluation

The proposed models were evaluated using a Monte Carlo simulation study with two goals. The first goal is to evaluate the model performance by examining the bias and the RMSE as defined in Table 1, as well as the empirical coverage for a nominal 95% confidence interval of each parameter of interest.

Table 1: Definition of Criteria Used for Model Evaluation (θ is a parameter)

Criteria	Definition
Bias	$Bias_{\hat{\theta}}(\hat{\theta}, \theta) = E_{\hat{\theta}}(\hat{\theta} - \theta)$
RMSE	$RMSE(\hat{\theta}) = \sqrt{E_{\hat{\theta}}(\hat{\theta} - \theta)^2}$

The second goal is to investigate the determinants of statistical power to detect between-person differences in the knot, which is achieved by conducting the likelihood ratio test (LRT) to compare two models without TICs to avoid the impact on the power of covariates. For this LRT, the reduced model specifies that $\boldsymbol{\Psi}$ has free variances and covariances of growth factors (i.e., the intercept and two slopes) but fixes the knot variance and the covariances between the knot and any latent variable. The full model, in contrast, estimates all ten parameters in the variance-covariance matrix $\boldsymbol{\Psi}$ of growth factors (i.e., the intercept, two slopes, and the knot). Accordingly, to test the null hypothesis that the knot variance is zero in the framework of BLSGM, the LRT with 4 degree of freedom relies on the knot variance and its covariances with any other growth factors. Each goal of the model evaluation was assessed using 1,000 replications with convergent solutions of both models. Table 2 lists all conditions which were carried out for the model evaluation.

3.1 Design of Simulation Study

As shown in Table 2, some parameters such as the intercept mean, the variance-covariance matrix of growth factors, and the width of the time-window of individual measurement occasions were the fixed conditions while others were

the manipulated conditions. We chose 6 and 10 as two different levels of the number of repeated measures: 6 was selected as the minimum number of the repeated measures to make the model fully identified³ while 10 was to allow for examination of the effect of increasing the number of measurement occasions. Moreover, for the study duration with 10 records, we assessed the effect of the knot location by investigating conditions with the midway knot, left-shifted knot, and right-shifted knot. Additionally, we investigated 3 levels of magnitude of true between-person difference in the knot: 0's are the conditions without considering the knot variance, under which we evaluated the size (i.e., the Type I error rate) of the LRT to detect knot variance; the other two are the scenarios with the knot variability, under which we investigated the statistical power of the LRT. We also considered two levels of sample size, six levels of Cohen's d_z ⁴, two levels of effects of exogenous variables on endogenous growth factors⁵, and two levels of measurement precision as such is shown in Table 2.

Table 2: Simulation Design for BLSGM-TICs with an Unknown Knot in the ITPs Framework

Fixed Conditions	
Variables	Conditions
Mean of the Intercept	$\mu_{\eta_0} = 100$
Variance of the Intercept	$\psi_{00} = 25$
Mean of the 1st Slope	$\mu_{\eta_1} = -5$
Variance of Slopes	$\psi_{11} = \psi_{22} = 1$
Correlations of Growth Factors	$\rho = 0.3$
Manipulated Conditions	
Partially Crossed Design	
Variables	Conditions
Time (t_j)	6 scaled and equally spaced ($j = 0 \dots, J - 1, J = 6$) 10 scaled and equally spaced ($j = 0, \dots, J - 1, J = 10$)
(Mean of) the knot	μ_{γ} at $t = 2.5$ for $J = 6$ μ_{γ} at $t = 3.5$ or 4.5 or 5.5 for $J = 10$
Individual t_{ij}	$t_{ij} \sim U(t_j - \Delta, t_j + \Delta)(j = 0, \dots, J - 1; \Delta = 0.25)$
Sample Size	$n = 200$ $n = 500$
Full Factorial Design	
Variables	Conditions
Cohen's d_z	$\mu_{\eta_1} - \mu_{\eta_2} = \pm 1.6$ (1.0-unit Cohen's d_z) $\mu_{\eta_1} - \mu_{\eta_2} = \pm 2.4$ (1.5-unit Cohen's d_z) $\mu_{\eta_1} - \mu_{\eta_2} = \pm 3.2$ (2.0-unit Cohen's d_z)
Variance of Knots	$\psi_{\gamma\gamma} = 0$ ($sd(\gamma)/(t_j - t_{j-1}) = 0$) $\psi_{\gamma\gamma} = 0.09$ ($sd(\gamma)/(t_j - t_{j-1}) = 0.3$) $\psi_{\gamma\gamma} = 0.36$ ($sd(\gamma)/(t_j - t_{j-1}) = 0.6$)
Coefficients (B)	TICs explain 13% variability of growth factors TICs explain 26% variability of growth factors
Residual Variance	$\theta_{\epsilon} = 1$ $\theta_{\epsilon} = 2$

3.2 Data Generation and Simulation Step

For each condition which is listed in Table 2, the general steps of the simulation study for the BLSGMs-TICs with an unknown knot in the ITPs framework were carried out as follows:

1. Generated data for growth factors and TICs simultaneously using the R package *MASS* (Venables and Ripley, 2002) (more details are provided in Supplementary 6.5).

³It has been proved that the bilinear latent growth model with a specified knot can be identified with at least five waves of data (Bollen and Curran, 2005).

⁴We borrowed this concept from behavioral science to account for the difference between the two slopes and viewed three magnitudes, 1-, 1.5-, and 2-unit as a relatively small-, medium-, and large-difference, respectively (Cohen, 1988). In the design, we used both positive and negative values of these quantities.

⁵We let the TICs explain moderate (13%) and substantial (26%) variances of such factors (Cohen, 1988).

2. Generated the time structure with J scaled and equally-spaced waves t_j and obtained ITPs: $t_{ij} \sim U(t_j - \Delta, t_j + \Delta)$ by allowing disturbances around each time point.
3. Calculated definition variables (i.e., factor loadings in our case) for each individual based on ITPs and the knot.
4. Calculated values of the repeated outcomes based on growth factors, factor loadings, and residual variances.
5. Implemented the BLSGMs-TICs with an unknown knot on simulated data, estimated the parameters, constructed corresponding 95% Wald CIs. Refit both models without TICs and compared them via LRT.
6. Replicated the above steps until after obtaining 1,000 convergent solutions.

4 Result

4.1 Preliminary Analysis

Table 3: Number of Improper Solutions among 1,000 Replications of the BLSGM-TICs in the ITPs Framework (Conditions with 10 Repeated Measures & Midway Knot, 13% Explained Variance)

		$\theta_\epsilon = 1$		$\theta_\epsilon = 2$		
		$n = 200$	$n = 500$	$n = 200$	$n = 500$	
Small Cohen's d_z	Positive d_z	$sd(\gamma) = 0$	555//48 ¹	516//22	550//40	507//29
		$sd(\gamma) = 0.3$	117//35	7//11	278//48	168//21
		$sd(\gamma) = 0.6$	4//3	0//0	58//25	7//6
	Negative d_z	$sd(\gamma) = 0$	535//37	542//27	568//44	531//27
		$sd(\gamma) = 0.3$	106//49	24//14	279//59	134//39
		$sd(\gamma) = 0.6$	0//8	0//0	67//45	8//17
Medium Cohen's d_z	Positive d_z	$sd(\gamma) = 0$	563//49	553//28	583//39	573//22
		$sd(\gamma) = 0.3$	17//14	1//0	141//27	40//11
		$sd(\gamma) = 0.6$	0//1	0//0	9//2	0//0
	Negative d_z	$sd(\gamma) = 0$	568//42	542//26	576//50	513//32
		$sd(\gamma) = 0.3$	19//17	1//0	130//64	22//32
		$sd(\gamma) = 0.6$	0//0	0//0	4//23	0//0
Large Cohen's d_z	Positive d_z	$sd(\gamma) = 0$	555//44	555//36	562//45	557//19
		$sd(\gamma) = 0.3$	1//0	0//0	27//19	0//0
		$sd(\gamma) = 0.6$	0//0	0//0	0//0	0//0
	Negative d_z	$sd(\gamma) = 0$	548//35	514//30	555//36	523//33
		$sd(\gamma) = 0.3$	1//2	0//0	37//39	2//6
		$sd(\gamma) = 0.6$	0//0	0//0	0//2	0//0

¹ 555//48 indicates that among 1,000 convergent replications of the BLSGM-TICs, we have 555 and 48 improper solutions due to negative knot variances and out-of-range correlations of the knot with other growth factors, respectively.

Before evaluating model performance, we first examined the convergence rate and component fit measures of each condition. The convergence⁶ rate of each condition was investigated. Based on our simulation studies, the proposed BLSGM-TICs and its reduced version converged satisfactorily (the convergence rate achieved 100% for $\sim 90\%$ conditions while at least 95% for other scenarios).

We also conducted diagnostics to investigate improper solutions, such as estimates of growth factor variances are less than 0, and/or estimates of correlations between growth factors are beyond $[-1, 1]$. Table 3 demonstrates the number of improper solutions yielded by the proposed model under conditions with 10 repeated measures, the midway knot, and 13% explained variance of the latent growth factors, which include negative knot variances and its out-of-range (i.e., out of $[-1, 1]$) correlations with any other growth factors. When the population value of the knot variance was 0 or relatively small (i.e., $sd(\gamma) = 0.3$), the number of improper solutions was relatively large.

For the scenarios including knots with variability, we observed that the proper solution rate has positive associations with the magnitude of Cohen's d_z , the measurement precision, the sample size, and the knot standard deviation. Negative Cohen's d_z (i.e., the second slope is less than the first slope as shown in the left panel of Figure 1) or positive

⁶In our project, convergence is defined as to achieve *OpenMx* status code 0, which suggests a successful optimization, until up to 10 attempts with different sets of starting values (Neale et al., 2016).

Cohen’s d_z seemed not to affect the number of improper solution meaningfully. We further noticed that the shifted knot locations or the proportion of explained variance of latent growth factors did not affect the rate of improper solution meaningfully but that reduced follow-up time inflated this number. When such improper solutions emerged, we replaced the BLSGM-TICs with its reduced version for the model evaluation.

4.2 Primary Analysis

4.2.1 Biases of Parameters of Interest

Table 4: Summary the Bias of Each Parameter in BLSGMs-TICs in the ITPs Framework of All Conditions

	Para.	Reduced BLSGM-TICs	Full BLSGM-TICs
		Median (Range)	Median (Range)
Mean Vector	μ_{η_0}	0.0004(−0.0858, 0.0821)	−0.0001(−0.0708, 0.0647)
	μ_{η_1}	0.0000(−0.1210, 0.1201)	0.0000(−0.1198, 0.1210)
	μ_{η_2}	0.0002(−0.1221, 0.1234)	0.0002(−0.1196, 0.1230)
	μ_{γ}	−0.0001(−0.0540, 0.0510)	0.0000(−0.0250, 0.0287)
Path Coef. of x_1	β_{10}	0.0014(−0.1132, 0.1025)	0.0008(−0.0472, 0.0378)
	β_{11}	0.0000(−0.1180, 0.1212)	0.0000(−0.0669, 0.0716)
	β_{12}	−0.0001(−0.1229, 0.1200)	−0.0001(−0.0634, 0.0620)
	$\beta_{1\gamma}$	−0.0641(−0.1502, 0.0000)	−0.0120(−0.1037, 0.0035)
Path Coef. of x_2	β_{20}	0.0002(−0.1352, 0.1366)	0.0004(−0.0460, 0.0597)
	β_{21}	0.0000(−0.1781, 0.1775)	−0.0001(−0.1029, 0.0997)
	β_{22}	0.0002(−0.1803, 0.1774)	0.0002(−0.1066, 0.0962)
	$\beta_{2\gamma}$	−0.0961(−0.2253, 0.0000)	−0.0185(−0.1565, 0.0033)
Unexplained Variance	ψ_{00}	−0.2229(−0.9849, 0.5176)	−0.2138(−0.6344, 0.0391)
	ψ_{11}	−0.0060(−0.0816, 0.3006)	−0.0088(−0.0737, 0.1457)
	ψ_{22}	−0.0066(−0.0873, 0.2978)	−0.0084(−0.0825, 0.1374)
	$\psi_{\gamma\gamma}$	−0.0724(−0.3132, 0.0000)	0.0017(−0.2041, 0.1033)

Table 4 presents the median and range of the bias (as defined in Table 1) for each parameter of interest across all conditions for the proposed BLSGM-TICs and its reduced version. We first calculated the bias of each parameter across 1,000 replications under each condition and then summarized the biases of each parameter over all the conditions as the bias median and range. As shown in Table 4, both models generated unbiased point estimates for the mean vector but relatively biased point estimates for the path coefficients given their population values. However, the ranges of biases of the parameters from the full model were narrower than those from the reduced model, especially for the path coefficients and corresponding unexplained variances of latent growth parameters, indicating that the full model yielded estimates which were closer to the population values generally.

We then further investigated the ‘essential’ factors to the bias of each parameter of each condition. Figure 2 plots the biases of the mean vector to further examine the impact on the mean vector biases of the Cohen’s d_z and the knot standard deviation as well as to compare two models. All panels plot the biases of parameters of the full model against those of the reduced model under conditions with 10 repeated measures, the midway knot, and 13% explained variance. We colored 0, 0.3 and 0.6 knot standard deviation in green, purple and red, respectively. We used circles, triangles and squares to represent small, medium and large Cohen’s d_z ’s, respectively. Additionally, we let solid and hollow shapes be positive Cohen’s d_z ’s and negative Cohen’s d_z ’s, respectively.

As shown in Figure 2, the magnitudes of biases of the mean vector produced by both models were small and comparable. It is noted that the biases were positively associated with the standard deviation of the knot and the Cohen’s d_z . Additionally, the biases of the intercept and two slopes were in opposite directions for the negative Cohen’s d_z ’s and positive Cohen’s d_z ’s. When comparing the bias patterns shown in Figure 2 to the other conditions with midway knot (i.e., the conditions with 6 repeated measures and $\mu_{\gamma} = 2.5$), we noticed that the reduced follow-up time increased the biases of the mean vector. When comparing the bias patterns among three scenarios with 10 repeated measures, we noted that the left-shifted knot inflated the bias of the first slope mean but deflated that of the second slope mean whereas the right-shifted knot affected the biases conversely. Moreover, the estimates of the non-center knots tended to shift towards the center of the study duration. Additionally, the proportion of variances of growth factors explained by TICs seemed not to affect the biases of the mean vector.

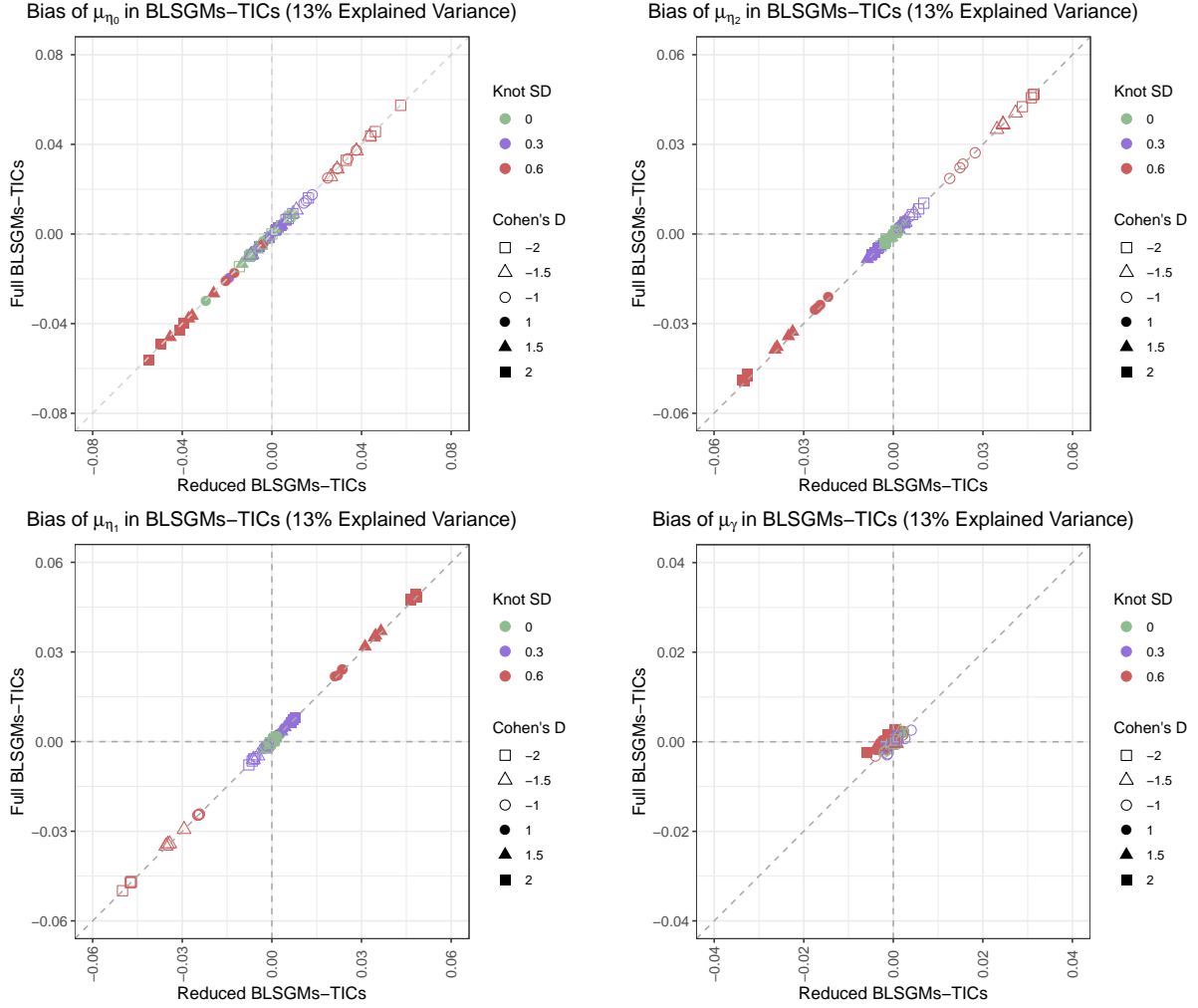


Figure 2: Biases of Mean Vector of Growth Factors of BLSGM-TICs with in the ITPs Framework (Under Conditions with 10 Repeated Measures, Midway Knot & 13% explained variance)

Figures 3, 4, 5 and 6 plot the biases of path coefficients and corresponding residuals of each growth factor to investigate the impact on biases of factors, such as the standard deviation of the knot, the Cohen’s d_z , and the proportion of the variance of growth factor which can be explained by TICs. The left and right panels are for conditions under which TICs can explain medium and substantial growth factor variances, respectively. For each plot, we employed the same color and shape schemes as we did in Figure 2.

Other than the bias patterns of the mean vector that we described in Figure 2, we noticed that the biases of the path coefficients and those of corresponding residuals exhibited sorts of ‘complementary’ relationship. For the intercept and two slopes, the biases of unexplained variances (i.e., residuals) reduced with the increased proportion of explained variances by TICs, and such shrinkages of the reduced model were faster than those of the full model until two models yielded comparable biases. Meanwhile, the biases which had belonged to the growth factor variances, ‘transferred’ to the corresponding path coefficients. In addition, we noticed that the unexplained variances of latent growth factors of the full model were biased downwards in general, which aligns with the results from the mixed-effects model via the maximum likelihood estimation technique (Hedeker and Gibbons, 2006).

When comparing the bias patterns shown in Figures 3, 4, 5 and 6 to the other conditions with 6 repeated measures and the midway knot, we noted that reduced follow-up time increased the biases of the path coefficients and corresponding unexplained variances of two slopes and that such increase was so evident for the residuals that the estimates of them were biased upwards. When comparing the bias patterns among three scenarios with 10 repeated measures, we observed

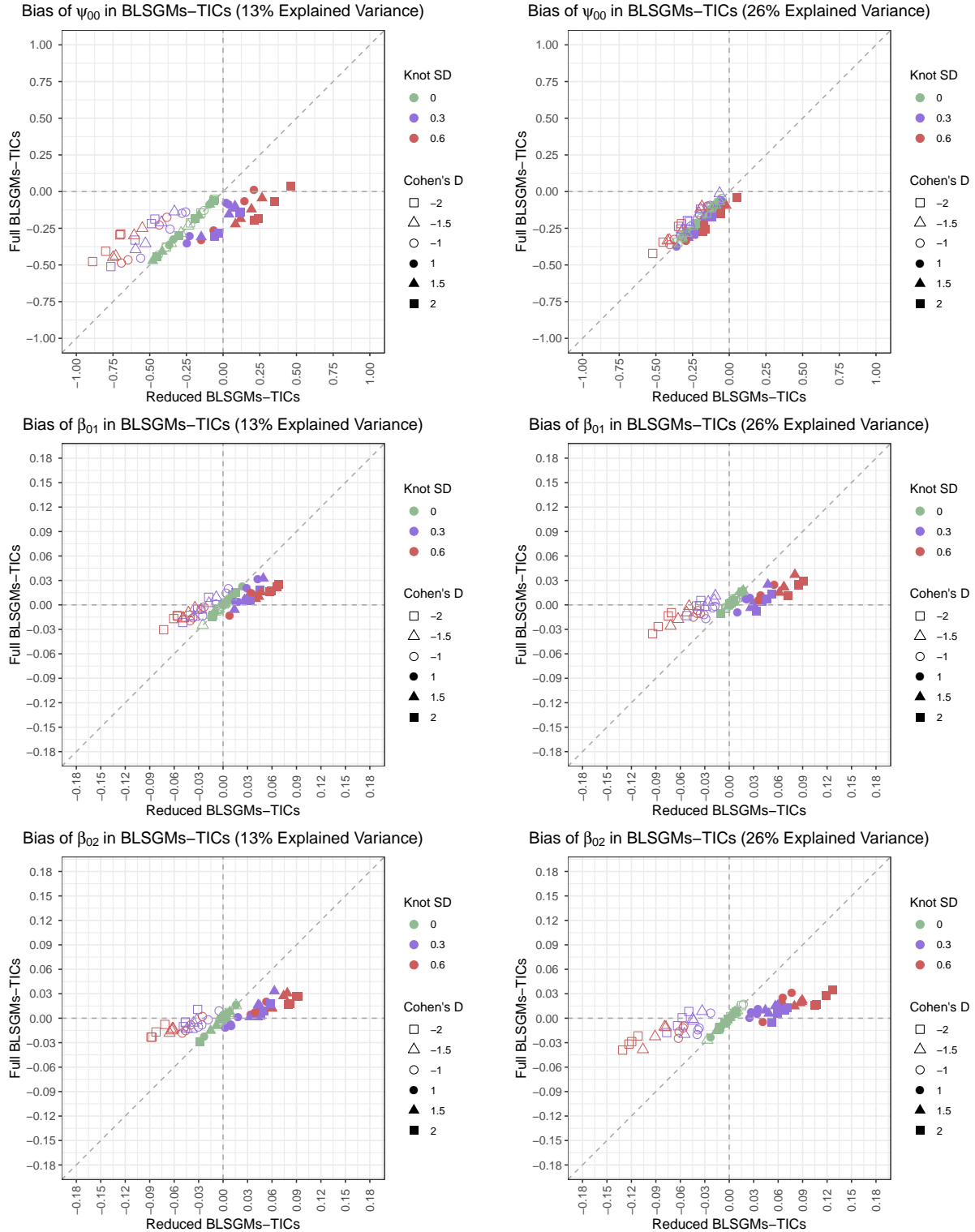


Figure 3: Biases of Path Coefficients and Residuals of Intercept of BLSGM-TICs with in the ITPs Framework (Under Conditions with 10 Repeated Measures, Midway Knot & 13% explained variance)

that the left-shifted knot worsened the performance of the first slope while the right-shifted knot decreased that of the second slope concerning of the biases of path coefficients and corresponding unexplained variances.

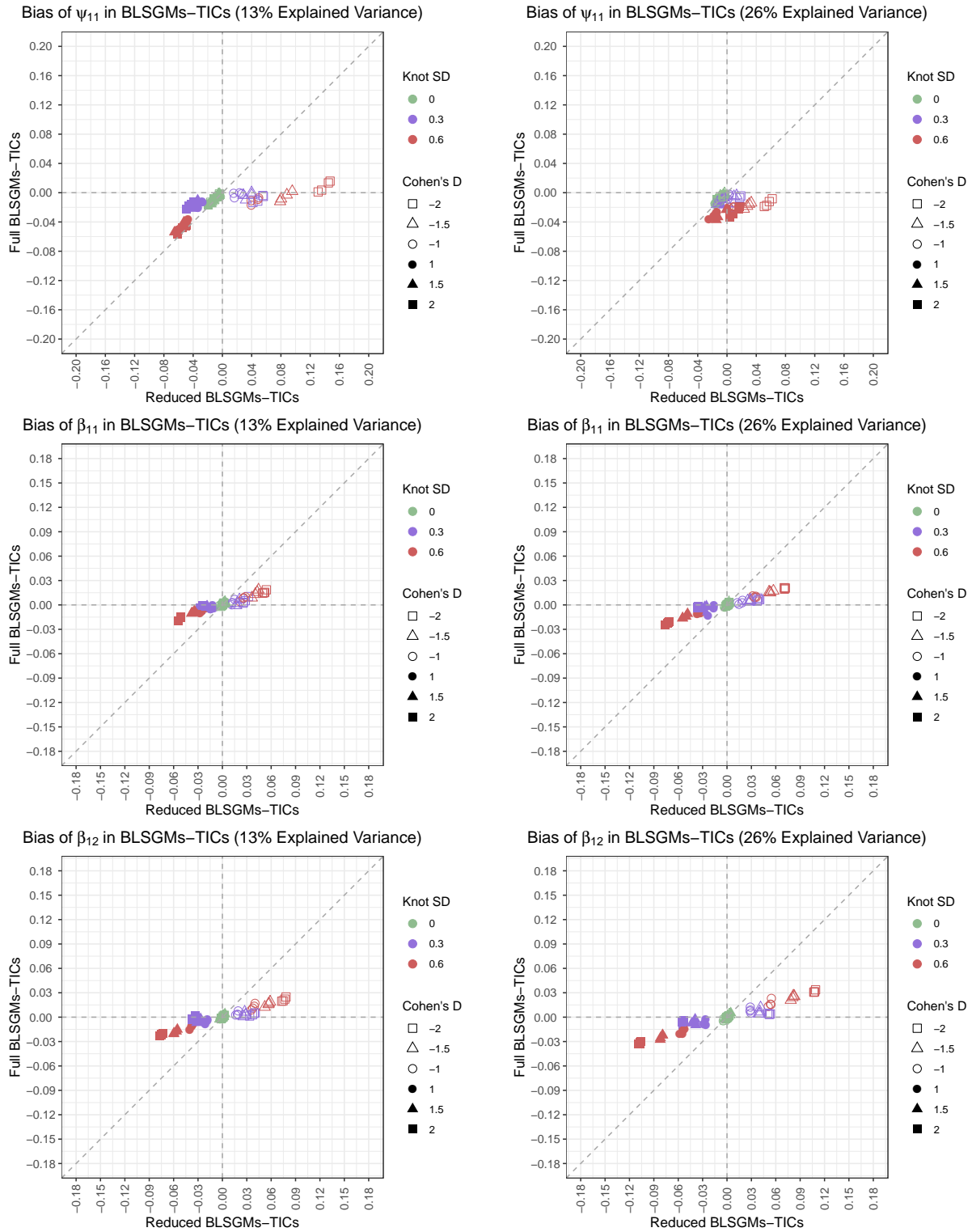


Figure 4: Biases of Path Coefficients and Residuals of 1st Slope of BLSGM-TICs with in the ITPs Framework (Under Conditions with 10 Repeated Measures & Midway Knot)

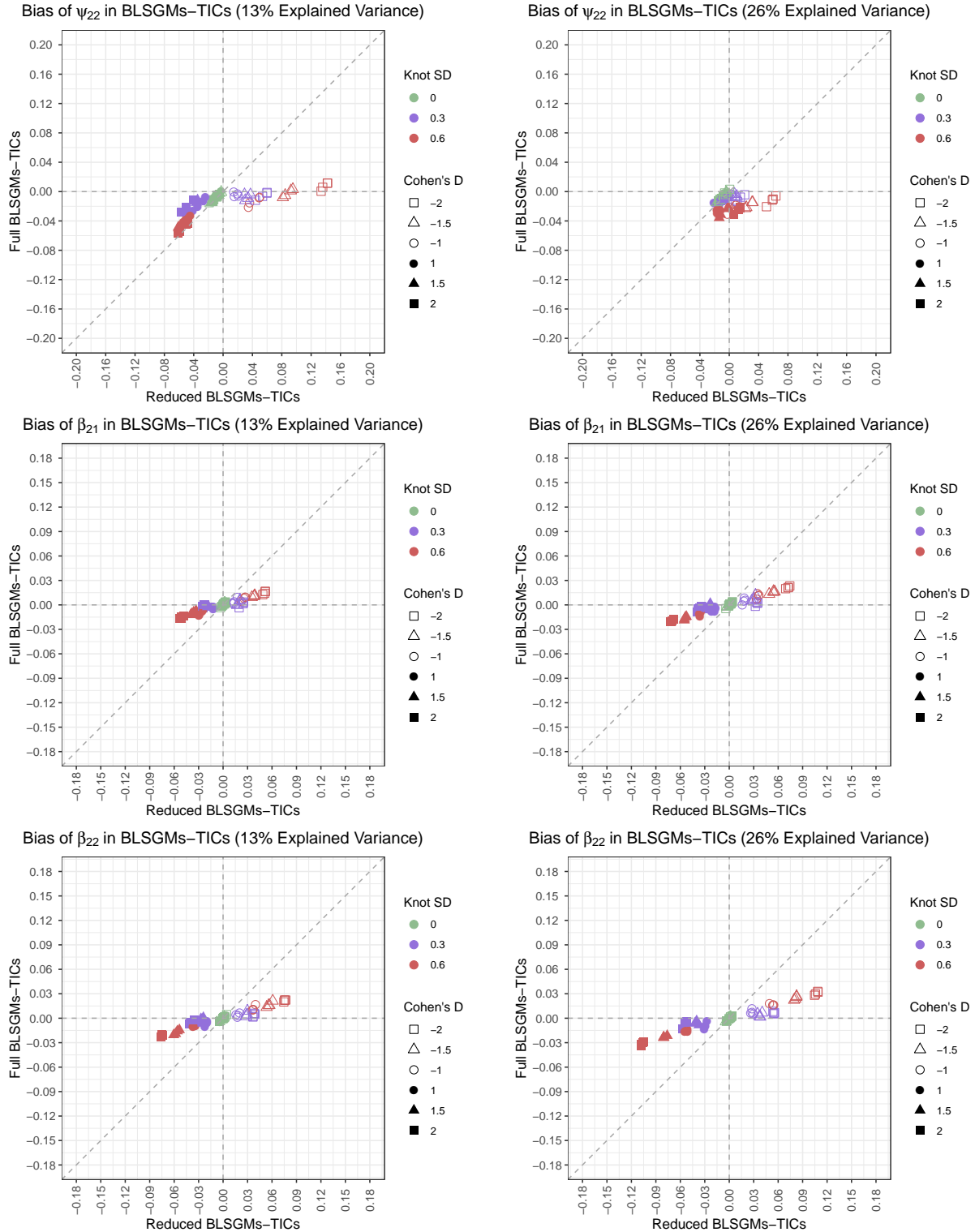


Figure 5: Biases of Path Coefficients and Residuals of 2nd Slope of BLSGM-TICs in the ITPs Framework (Under Conditions with 10 Repeated Measures & Midway Knot)

4.2.2 RMSE of Parameters of Interest

The median and range of RMSE (as defined in Table 1) for each parameter of interest across all conditions for both BLSGMs-TICs are shown in Table 5. Based on the examination of Table 5, it seemed that the size of the median and

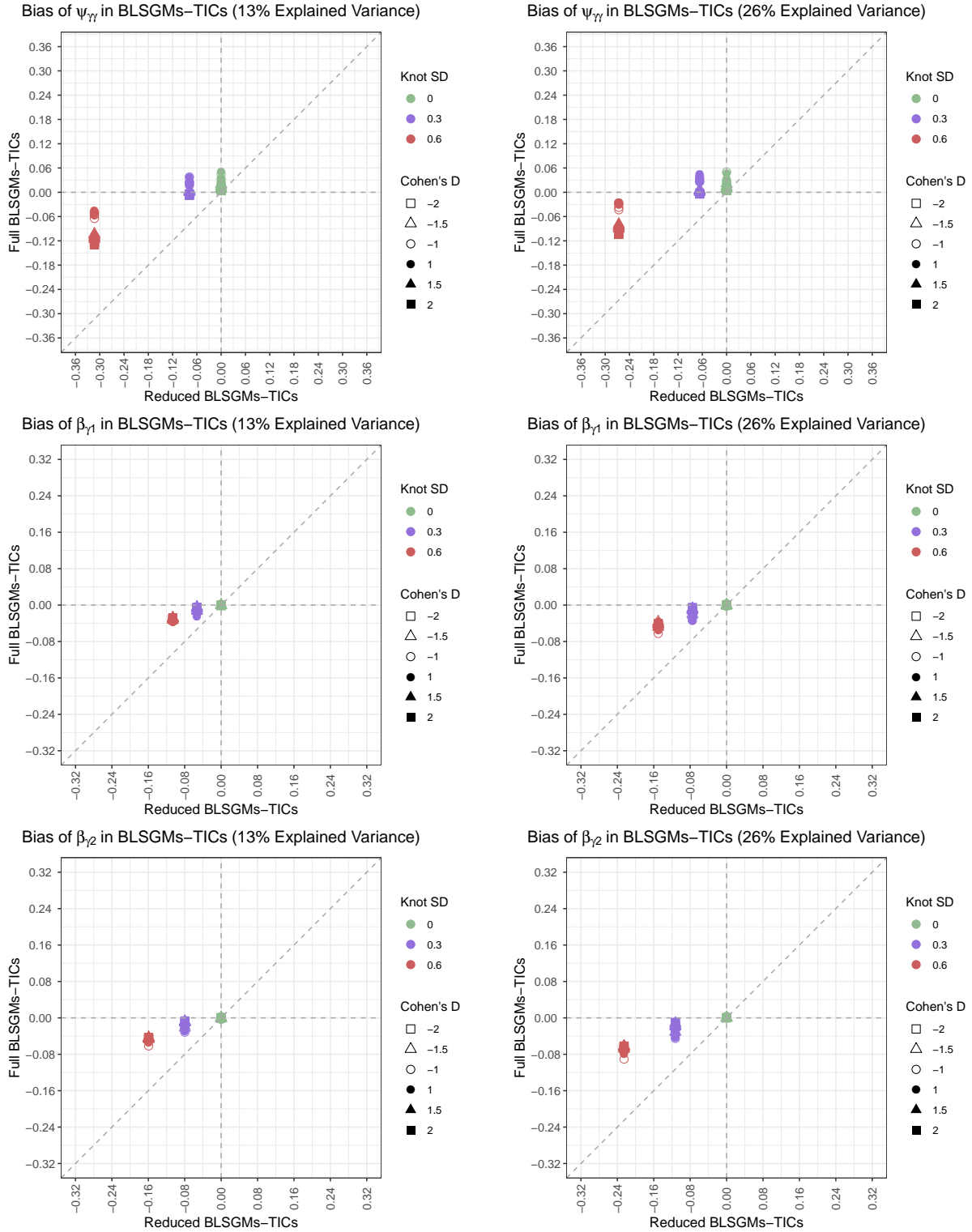


Figure 6: Biases of Path Coefficients and Residuals of Knot for BLSGM-TICs with in the ITPs Framework (Under Conditions with 10 Repeated Measures & Midway Knot)

range of RMSE was smaller for the estimates obtained from the full BLSGM-TICs, especially for the estimates of the

path coefficients and the unexplained variances. On further investigation, the reduced BLSGM-TICs seemed to estimate the mean vector, the path coefficients, and the unexplained variances as precisely as the proposed full BLSGM-TICs.

The RMSE of each parameter of interest demonstrated a similar association with Cohen’s d_z as well as the knot standard deviation as the bias. Specifically, it positively related to the magnitude of Cohen’s d_z and the knot standard deviation. In addition, it showed a negative association with sample size but a positive association with measurement precision.

Table 5: Summary the RMSE of Each Parameter in BLSGMs-TICs in the ITPs Framework of All Conditions

	Para.	Reduced BLSGM-TICs	Full BLSGM-TICs
		Median (Range)	Median (Range)
Mean Vector	μ_{η_0}	0.2618(0.1850, 0.3665)	0.2620(0.1853, 0.3632)
	μ_{η_1}	0.0665(0.0387, 0.1547)	0.0668(0.0386, 0.1552)
	μ_{η_2}	0.0668(0.0382, 0.1594)	0.0670(0.0382, 0.1585)
	μ_{γ}	0.0471(0.0166, 0.1085)	0.0455(0.0168, 0.1082)
Path Coef. of x_1	β_{10}	0.2700(0.1969, 0.3811)	0.2692(0.1967, 0.3769)
	β_{11}	0.0711(0.0411, 0.1516)	0.0670(0.0412, 0.1254)
	β_{12}	0.0714(0.0410, 0.1517)	0.0670(0.0410, 0.1262)
	$\beta_{1\gamma}$	0.0641(0.0000, 0.1502)	0.0488(0.0119, 0.1450)
Path Coef. of x_2	β_{20}	0.2824(0.1979, 0.3851)	0.2768(0.1981, 0.3823)
	β_{21}	0.0752(0.0395, 0.2023)	0.0688(0.0398, 0.1533)
	β_{22}	0.0758(0.0401, 0.1996)	0.0683(0.0405, 0.1529)
	$\beta_{2\gamma}$	0.0961(0.0000, 0.2253)	0.0542(0.0115, 0.1928)
Unexplained Variances	ψ_{00}	1.7210(1.1470, 2.4947)	1.6779(1.1541, 2.4676)
	ψ_{11}	0.0883(0.0484, 0.3407)	0.0874(0.0491, 0.2619)
	ψ_{22}	0.0875(0.0472, 0.3374)	0.0876(0.0478, 0.2532)
	ψ_{22}	0.0724(0.0000, 0.3132)	0.0646(0.0068, 0.2816)

4.2.3 Coverage Probabilities of Parameters of Interest

Figure 7 shows the coverage probabilities (CPs) of the mean vector of latent growth parameters based on 1,000 Monte Carlo replications under conditions with 10 repeated measurements, the midway knot, and 13% explained variances. The left-hand panels and right-hand panels are for positive and negative Cohen’s d_z , respectively. All figures depict the CP as a function of the knot standard deviation. In each plot, green and purple lines are for the sample size of 200 and 500, respectively; solid, short-dashed, and long-dashed lines are for the small-, medium-, and large-Cohen’s d_z between two slopes, respectively.

As shown in Figure 7, both models exhibited proper CPs (i.e., the CPs were around 0.95) when the population value of the knot variance was 0 while the full model covered better under the other conditions. In the non-zero knot standard deviation scenarios, we also noticed that the nominal confidence intervals were associated with factors such as the sample size and Cohen’s d_z . Additionally, the sign of the difference between two slopes seemed not to affect the CPs of the mean vector of the growth parameters meaningfully. Comparing the CPs shown in Figure 7 with those under conditions with 6 repeated measurements and a midway knot, we observed that the reduced model covered worse for two slope means but better for the knot mean. Among scenarios with 10 repeated measures, the left-shifted knot lowered the performance of the first slope but enhanced the performance of the second slope in terms of CPs; the right-shifted knot performed oppositely. The increased proportion of explained variance did not change the CPs of the mean vector meaningfully.

Concerning the path coefficients of latent growth parameters, as shown in Figures 8 and 9, we perceived similar patterns of CPs as we did for those of the mean vector except that the performance of coverage probability reduced when the level of explained variance was higher. Additionally, it seemed that the CPs of unexplained variances yielded by the reduced BLSGM-TICs, as shown in Figure 10, covered the population values of the residuals of two slopes better under the conditions with positive Cohen’s d_z than they did in the negative Cohen’s d_z scenarios.

4.2.4 Statistical Power to Detect Between-Person Differences in the Knot

Figure 11 plots the simulation results of the statistical power of the LRTs with 4 degree-of-freedom based on 1,000 Monte Carlo replications of each condition with 10 repeated measures and the midway knot. Each panel plots the power

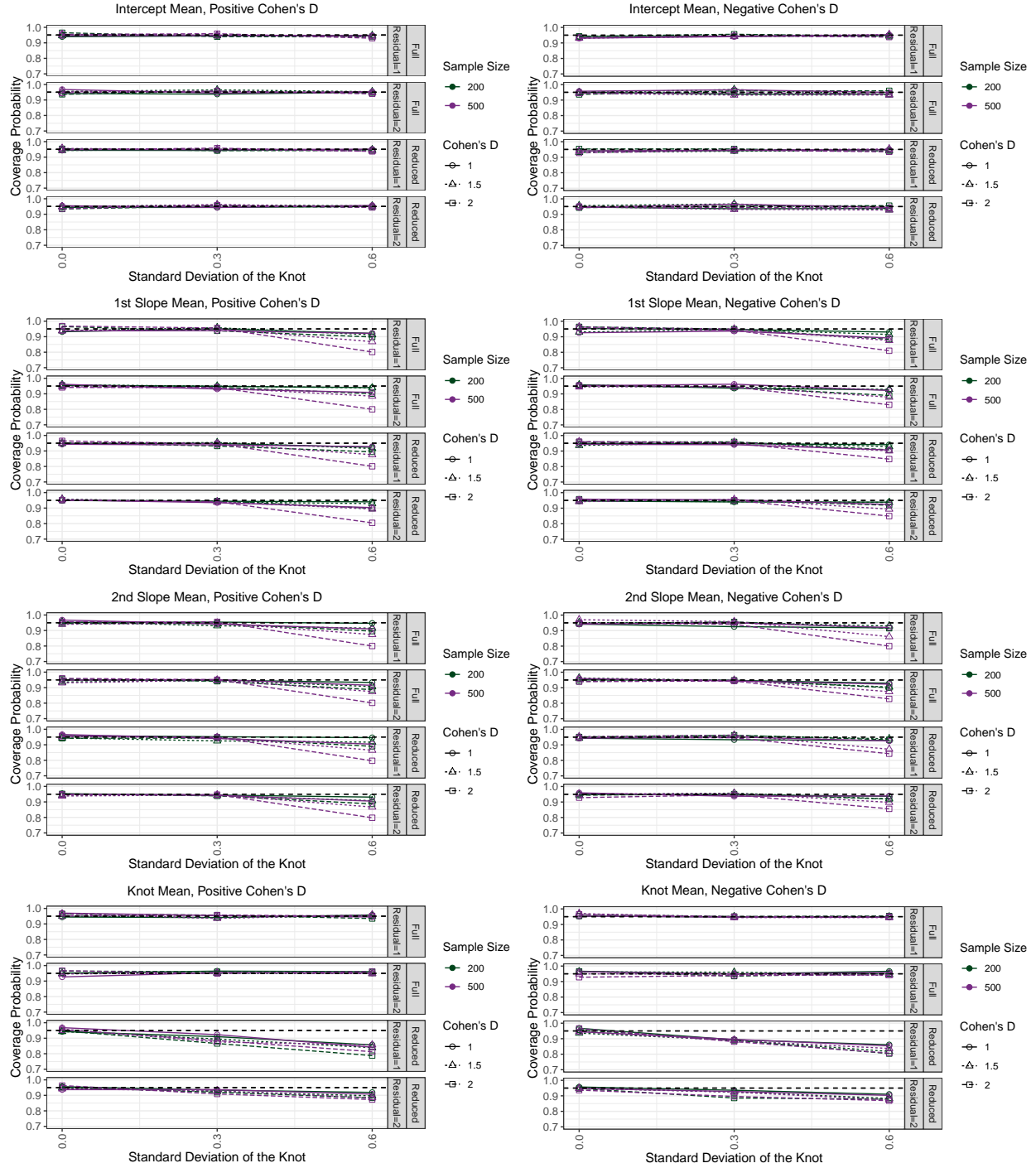


Figure 7: Coverage Probability of Means of Latent Variables in BLSGMs-TICs in the ITPs Framework (Under Conditions with 10 Repeated Measures Midway Knot, & 13% Explained Variance)

as a function of the varying knot standard deviation: the left and right panels are for conditions with small residual variances and large residual variances, respectively. The top panels and the bottom panels are for the positive and negative Cohen's d_z , respectively. We employed the same color and shape/line schemes as we did in Figure 7.

As shown in Figure 11, the LRTs controlled well for the Type I error rate since the size of the test of each condition without considering the knot variance was around 0.05. It was also noted that factors such as the magnitude of the

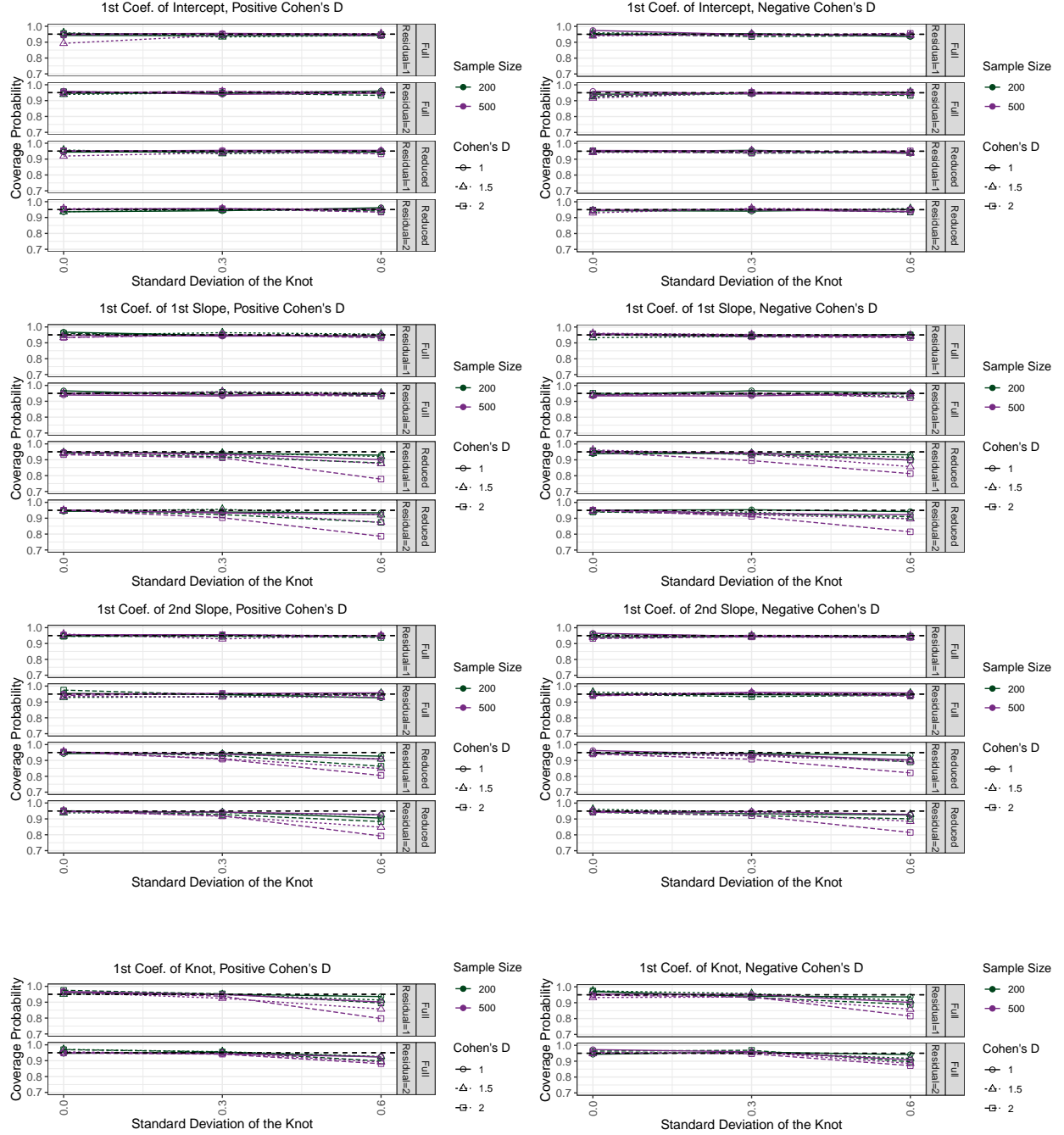


Figure 8: Coverage Probability of Path Coefficients of x_1 in BLSGMs-TICs in the ITPs Framework (Under Conditions with 10 Repeated Measures, Midway Knot, Small Residuals & 13% Variances Explained by TICs)

population value of between-person differences in the knot, the Cohen's d_z between two slopes, the precision of measurements, and the sample size were the primary determinants of the statistical power to detect the zero knot variance. Specifically, the statistical power had positive associations with the true value of the knot variance, the sample size, the magnitude of Cohen's d_z between two slopes, and the precision of measures (i.e., the power has a negative relationship with the residual variance). We also noticed that the power of conditions with negative Cohen's d_z was slightly larger than those with positive Cohen's d_z . Comparing to the statistical power of condition factors not

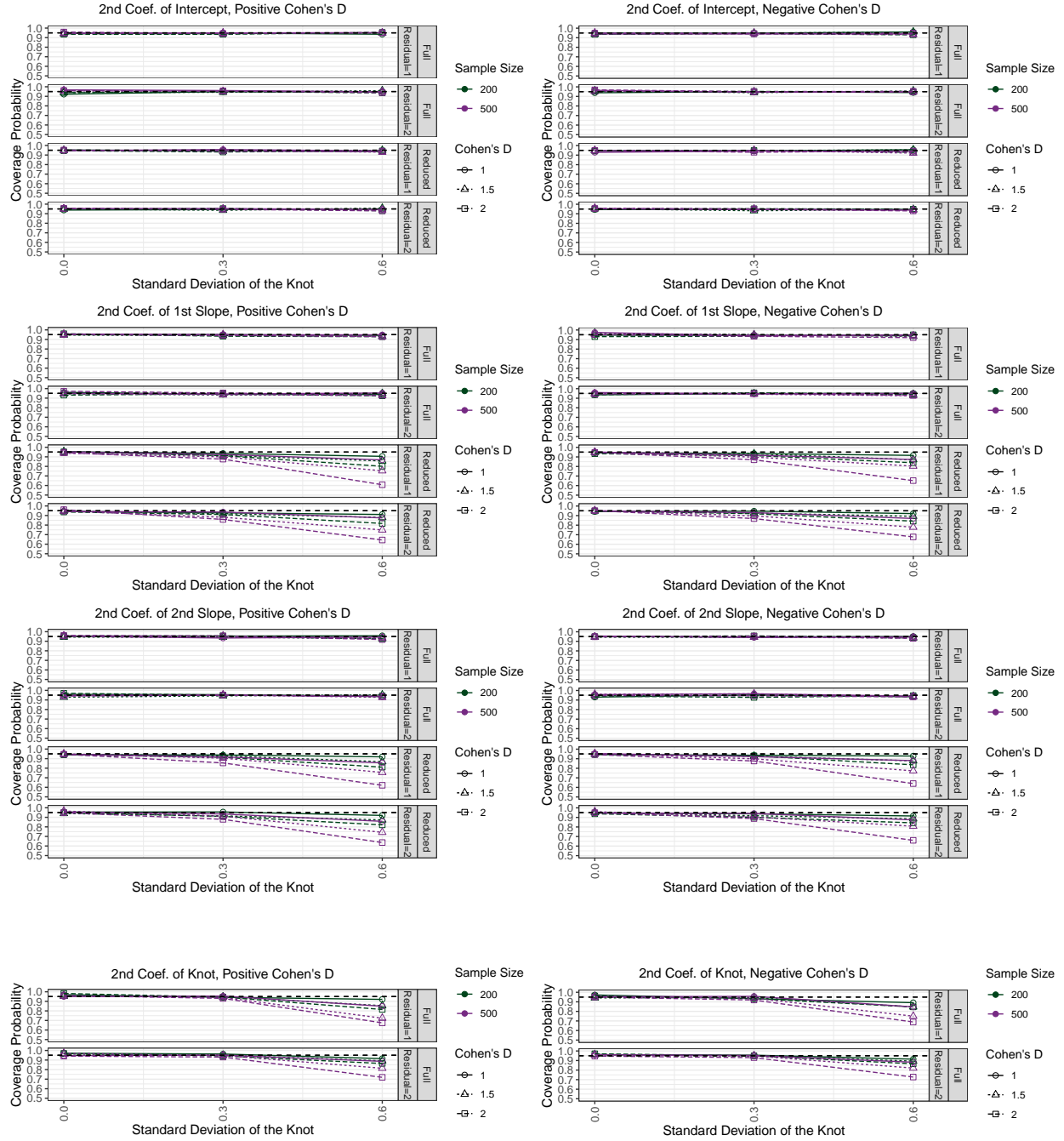


Figure 9: Coverage Probability of Path Coefficients of x_2 in BLSGMs-TICs in the ITPs Framework (Under Conditions with 10 Repeated Measures, Midway Knot, Small Residuals & 13% Variances Explained by TICs)

distinguished in the figures, we learned that non-center knot locations did not affect the statistical power meaningfully, but that reduced number of repeated measures decreased the statistical power.

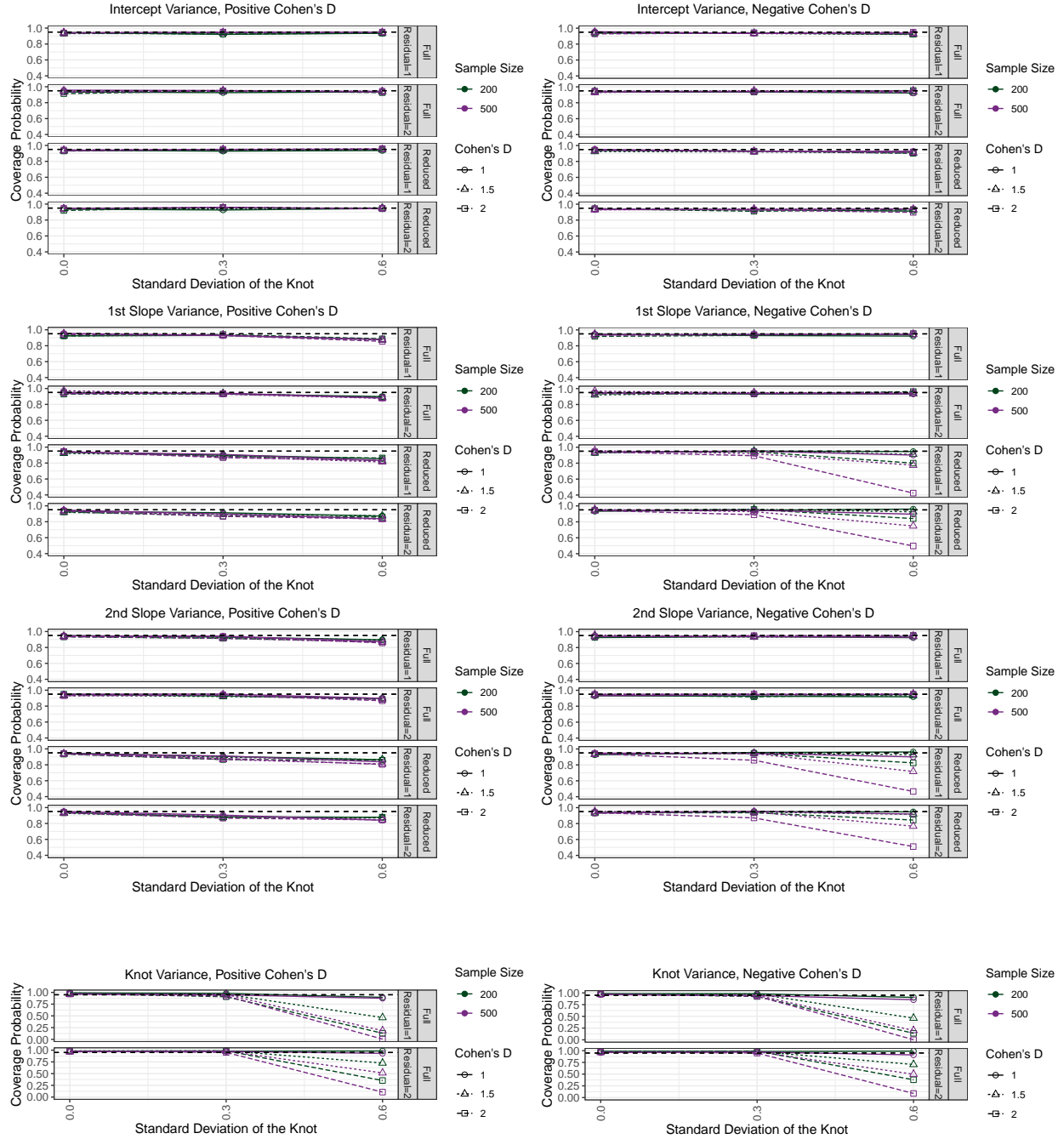


Figure 10: Coverage Probability of Variances of Latent Variables in BLSGMs-TICs in the ITPs Framework (Under Conditions with 10 Repeated Measures Midway Knot, & 13% Explained Variance)

5 Discussion

We developed a pair of BLSGMs-TICs for estimating an inflection point in the framework of individual measurement occasions. In both models, we viewed characteristics of the knot—its location and spread—as parameters to provide a more flexible approach to examine piecewise linear-linear change patterns. The proposed full BLSGM-TICs allows us to estimate the location of the knot rather than pre-specify it and then examine the predictors of the between-individual

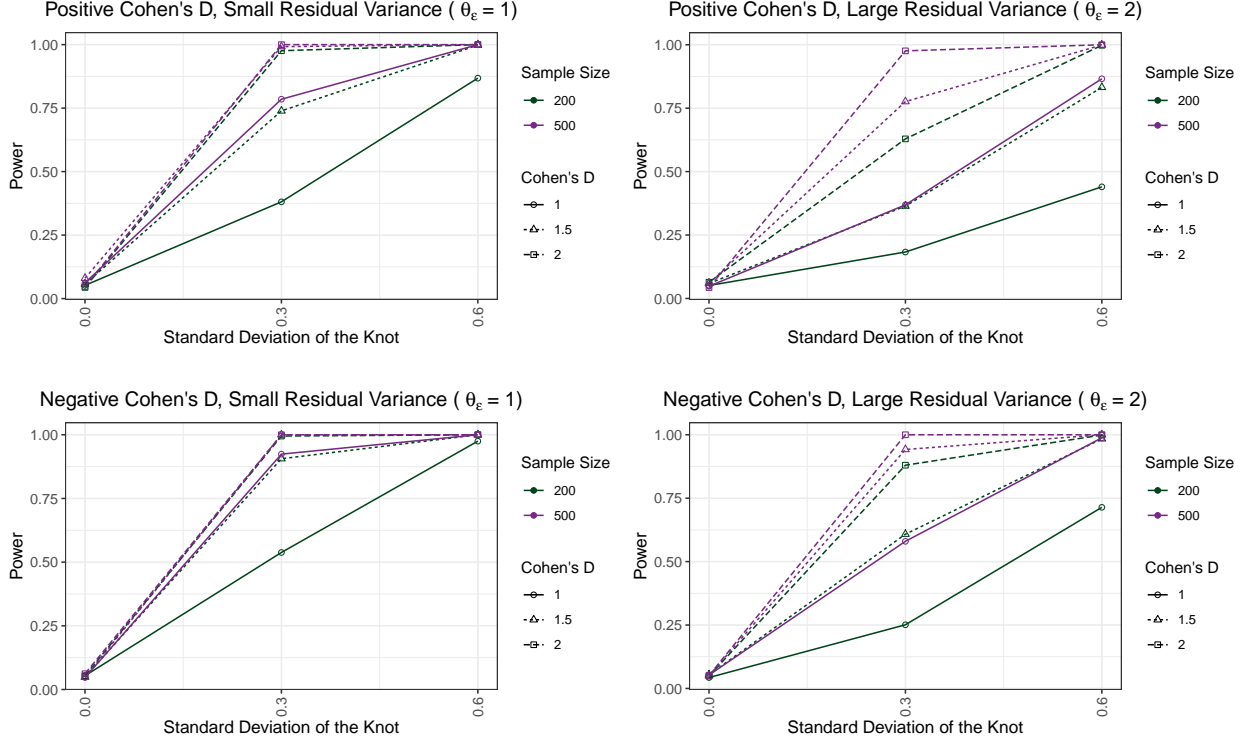


Figure 11: Statistical Power of LRTs to Test Zero Knot Variance in BLSGMs in the ITPs Framework (Under Conditions with 10 Repeated Measures & Midway Knot)

differences in the knot. Its reduced version provides a parsimonious option for the scenario in which such between-person differences in the knot are not significant. More importantly, we performed in-depth analyses concerning the non-convergent rate, improper solutions, statistical power to detect the variability of the knot, as well as the bias, RMSE, and coverage probability of each parameter through simulation studies.

Across all conditions that we considered in the simulation design, both models converged satisfactorily—the convergence rate of the full BLSGM-TICs achieved 100% for $\sim 90\%$ conditions while at least 95% for others while the rate of the reduced BLSGM-TICs was always 100%. Accordingly, in real practice, we recommend employing the reduced version if the full model fails to converge, though it is rare.

Of the 1,000 replications with convergent solutions across all conditions, we first examined the rate of improper solutions. Under the conditions with zero knot standard deviation, the full BLSGM-TICs suffered the improper solution issue: either negative knot variances or out-of-range correlations of the knot with other growth factors (i.e., the intercept and two slopes). It is not surprising since the full model was misspecified under the ‘true’ fixed knot conditions. Accordingly, we recommend employing the reduced BLSGM-TICs, which only estimates the knot itself, if improper solutions emerge when analyzing real-world data.

We then evaluated models based on the replications with convergent solutions concerning the point estimate and the coverage probability of each parameter of interest. Generally, the reduced BLSGM-TICs with an unknown knot performed well and generated desirable point estimates and coverage probabilities under the conditions without considering the knot variance. In contrast, the full BLSGM-TICs for estimating a knot and its variance, which generally performed better than the reduced model concerning point estimates and coverage probabilities in the other scenarios, were capable of yielding unbiased and precise point estimates and appropriate coverage probability. Additionally, increased follow-up time enhanced the performance of both models in general; the left-shifted knot made the estimates of the parameters of the first slope (i.e., the mean and variance of the first slope) worse but those of the second slope (i.e., the mean and variance of the second slope) better while the right-shifted knot worked oppositely.

Moreover, of the reduced BLSGM-TICs, the bias of coefficients and that of corresponding unexplained factor variance exhibited a ‘complementary’ pattern: the bias which had belonged to the growth factor variance shifted to the corresponding path coefficients, and such transfer was more evident in the scenarios under which TICs can explain a

higher proportion of between-individual differences in the growth factors. However, this pattern was less noticeable for the full BLSGM-TICs.

In addition, we noticed that the unexplained growth factor variances of the full model were underestimated generally, which could either be the results of employing the maximum likelihood estimation approach or be the consequence of the approximation introduced by the Taylor series expansion and the inverse-transformed matrices of the population-level. The biased upward estimates of unexplained growth factor variances of the reduced model under the condition with a random knot could be simply due to the model misspecification.

Additionally, we did notice several ‘unusual’ patterns of the coverage probabilities (CPs) of parameters. For example, the CPs of the estimates of the mean vector and the variance-covariance matrix seemed better under the conditions with the larger residual variance. However, it did not suggest that the models worked better when the measurement precision is relatively low. In contrast, the ‘better’ coverage probability resulted from the larger overestimated model-based standard errors (SEs) of parameters, which might result from the lower precision of measurements. Other than the model-based SE, the point estimate also affected the CPs. For instance, the better coverage of the model for estimating fixed knot under the conditions with the positive Cohen’s d_z ’s was the result of less biased point estimates.

We also examined the statistical power to detect the between-person differences in the inflection point. Under the conditions without considering the knot variability, the LRT controlled well for the Type I error rate. In the scenarios with a random knot, we observed that the statistical power demonstrated associations with multiple factors. Specifically, the power was positively associated with the sample size, the magnitude of Cohen’s d_z , the population value of the knot variance, and the measurement precision. Accordingly, when analyzing a real-world data set, we recommend fitting both BLSGMs, selecting the more suitable one based on such statistical criteria as well as the research question, and then building a model with considering TICs to explain the growth factor variances.

One limitation of this project lies in that we introduced approximations when replacing the individual-level inverse-transformed matrices with the population-level inverse-transformed matrices. As presented in Supplementary 6.2, the closer the knot variance is to 0, the better the approximations work. This partly explains why the model performance decreased with an increased knot standard deviation in the full model. However, it is noted that the full model still performed better than the reduced model, even with such approximations. Accordingly, we recommend employing the population-level inverse-transformed matrices to simplify the estimation process in practice.

References

- Boker, S. M., Neale, M. C., Maes, H. H., Wilde, M. J., Spiegel, M., Brick, T. R., Estabrook, R., Bates, T. C., Mehta, P., von Oertzen, T., Gore, R. J., Hunter, M. D., Hackett, D. C., Karch, J., Brandmaier, A. M., Pritikin, J. N., Zahery, M., Kirkpatrick, R. M., Wang, Y., Driver, C., Massachusetts Institute of Technology, Johnson, S. G., Association for Computing Machinery, Kraft, D., Wilhelm, S., Manjunath, B. G., 2018. OpenMx 2.9.6 User Guide.
- Bollen, K. A., Curran, P. J., 2005. Latent Curve Models. John Wiley & Sons, Inc.
- Browne, M. W., du Toit, S. H. C., 1991. Models for learning data. In: Collins, L. M., Horn, J. L. (Eds.), Best methods for the analysis of change: Recent advances, unanswered questions, future directions. American Psychological Association., Washington, DC, US, Ch. 4, pp. 47–68.
- Cohen, J., 1988. Statistical Power Analysis for the Behavioral Sciences (2nd Ed.). Lawrence Erlbaum Associates.
- Dumenci, L., Perera, R. A., Keefe, F. J., Ang, D. C., J., S., Jensen, M. P., Riddle, D. L., 2019. Model-based pain and function outcome trajectory types for patients undergoing knee arthroplasty: a secondary analysis from a randomized clinical trial. *Osteoarthritis and cartilage* 27 (6), 878–884.
- Finkel, D., Reynolds, C., Mcardle, J., Gatz, M., L Pedersen, N., 06 2003. Latent growth curve analyses of accelerating decline in cognitive abilities in late adulthood. *Developmental psychology* 39, 535–550.
- Flora, D. B., 2008. Specifying piecewise latent trajectory models for longitudinal data. *Structural Equation Modeling: A Multidisciplinary Journal* 15 (3), 513–533.
- Grimm, K. J., Ram, N., Estabrook, R., 2016. Growth Modeling. Guilford Press.
- Harring, J. R., 2009. A nonlinear mixed effects model for latent variables. *Journal of Educational and Behavioral Statistics* 34 (3), 293–318.
- Harring, J. R., Cudeck, R., du Toit, S. H. C., 2006. Fitting partially nonlinear random coefficient models as sems. *Multivariate Behavioral Research* 41 (4), 579–596.
- Hedeker, D., Gibbons, R. D., 2006. Longitudinal Data Analysis. Wiley Series in Probability and Statistics. Wiley.

- Hedeker, D., Mermelstein, R. J., Flay, B. R., 2006. Application of item response theory models for intensive longitudinal data. In: Walls, T. A., Schafer, J. L. (Eds.), *Models for Intensive Longitudinal Data*. Oxford University Press, ProQuest Ebook Central, Ch. 4, pp. 84–108.
- Hoyle, R. H., 2012. *Handbook of Structural Equation Modeling*. Guilford Press.
- Hunter, M. D., 2018. State space modeling in an open source, modular, structural equation modeling environment. *Structural Equation Modeling* 25 (2), 307–324.
- Jones, H. E., Bayley, N., 1941. The berkeley growth study. *Child Development* 12, 167–173.
- Kohli, N., 2011. Estimating unknown knots in piecewise linear-linear latent growth mixture models. Ph.D. thesis, University of Maryland.
- Kohli, N., Harring, J. R., Hancock, G. R., 2013. Piecewise linear-linear latent growth mixture models with unknown knots. *Educational and Psychological Measurement* 73 (6), 935–955.
- Kwok, O., Luo, W., West, S. G., 2010. Using modification indexes to detect turning points in longitudinal data: A monte carlo study. *Structural Equation Modeling: A Multidisciplinary Journal* 17 (2), 216–240.
- Mehta, P. D., Neale, M. C., 2005. People are variables too: Multilevel structural equations modeling. *Psychological Methods* 10 (3), 259–284.
- Mehta, P. D., West, S. G., 2000. Putting the individual back into individual growth curves. *Psychological Methods* 5 (1), 23–43.
- Neale, M. C., Hunter, M. D., Pritikin, J. N., Zahery, M., Brick, T. R., Kirkpatrick, R. M., Estabrook, R., Bates, T. C., Maes, H. H., Boker, S. M., 2016. OpenMx 2.0: Extended structural equation and statistical modeling. *Psychometrika* 81 (2), 535–549.
- Preacher, K. J., Hancock, G. R., 2015. Meaningful aspects of change as novel random coefficients: A general method for reparameterizing longitudinal models. *Psychological Methods* 20 (1), 84–101.
- Pritikin, J. N., Hunter, M. D., Boker, S. M., 2015. Modular open-source software for Item Factor Analysis. *Educational and Psychological Measurement* 75 (3), 458–474.
- Riddle, D. L., Perera, R. A., Jiranek, W. A., Dumenci, L., 2015. Using surgical appropriateness criteria to examine outcomes of total knee arthroplasty in a united states sample. *Arthritis care & research*. 67 (3), 349–357.
- Seber, G. A. F., Wild, C. J., 2003. *Nonlinear Regression*. John Wiley & Sons, Inc.
- Sterba, S. K., 2014. Fitting nonlinear latent growth curve models with individually varying time points. *Structural Equation Modeling: A Multidisciplinary Journal* 21 (4), 630–647.
- Tishler, A., Zang, I., 01 1981. A maximum likelihood method for piecewise regression models with a continuous dependent variable. *Journal of the Royal Statistical Society. Series C. Applied Statistics* 30.
- Venables, W. N., Ripley, B. D., 2002. *Modern Applied Statistics with S*, 4th Edition. Springer, New York.

6 Appendix

6.1 Taylor Series Expansion

For the i^{th} individual, suppose we have a function $f(\gamma_i)$ and its first derivative with respect to γ_i ⁷, shown in equations

$$f(\gamma_i) = \eta'_{0i} + \eta'_{1i}(t_{ij} - \gamma_i) + \eta'_{2i}\sqrt{(t_{ij} - \gamma_i)^2}$$

and

$$f'(\gamma_i) = \eta_{1i} - \eta'_{1i} - \frac{\eta'_{2i}(t_{ij} - \gamma_i)}{\sqrt{(t_{ij} - \gamma_i)^2}} = -\eta'_{2i} - \frac{\eta'_{2i}(t_{ij} - \gamma_i)}{\sqrt{(t_{ij} - \gamma_i)^2}},$$

respectively. Then the Taylor series expansion of $f(\gamma_i)$ can be expressed as

$$\begin{aligned} f(\gamma_i) &= f(\mu_\gamma) + \frac{f'(\mu_\gamma)}{1!}(\gamma_i - \mu_\gamma) + \dots \\ &= \eta'_{0i} + \eta'_{1i}(t_{ij} - \mu_\gamma) + \eta'_{2i}\sqrt{(t_{ij} - \mu_\gamma)^2} + (\gamma_i - \mu_\gamma) \left[-\eta'_{2i} - \frac{\eta'_{2i}(t_{ij} - \mu_\gamma)}{|t_{ij} - \mu_\gamma|} \right] + \dots \\ &\approx \eta'_{0i} + \eta'_{1i}(t_{ij} - \mu_\gamma) + \eta'_{2i}|t_{ij} - \mu_\gamma| + (\gamma_i - \mu_\gamma) \left[-\mu_{\eta'_2} - \frac{\mu_{\eta'_2}(t_{ij} - \mu_\gamma)}{|t_{ij} - \mu_\gamma|} \right], \end{aligned}$$

from which we then have the reparameterized growth factors and the corresponding factor loadings for the i^{th} individual.

6.2 Derivation of transformed matrices and the inverse-transformed matrices between mean vectors and variance-covariance matrices at the population-level

Through straightforward algebra, we can approximate the mean vector of the reparameterized growth factors from the mean vector of their original setting via the following equation

$$\begin{aligned} \boldsymbol{\mu}_{\eta'} &= E(\mathbf{G}_i \times \begin{pmatrix} \eta_{0i} \\ \eta_{1i} \\ \eta_{2i} \\ \gamma_i - \mu_\gamma \end{pmatrix}) = E \left[\begin{pmatrix} 1 & \gamma_i & 0 & 0 \\ 0 & 0.5 & 0.5 & 0 \\ 0 & -0.5 & 0.5 & 0 \\ 0 & 0 & 0 & 1 \end{pmatrix} \times \begin{pmatrix} \eta_{0i} \\ \eta_{1i} \\ \eta_{2i} \\ \gamma_i - \mu_\gamma \end{pmatrix} \right] \\ &\approx \begin{pmatrix} 1 & \mu_\gamma & 0 & 0 \\ 0 & 0.5 & 0.5 & 0 \\ 0 & -0.5 & 0.5 & 0 \\ 0 & 0 & 0 & 1 \end{pmatrix} \times \begin{pmatrix} \mu_{\eta_0} \\ \mu_{\eta_1} \\ \mu_{\eta_2} \\ 0 \end{pmatrix} \end{aligned}$$

under the condition of $\frac{1}{n} \sum_{i=1}^n Cov(\eta_{1i}, \gamma_i) \rightarrow 0$.

Similarly, the mean vector of the original parameters can be approximated from the reparameterized setting through the equation

$$\begin{aligned} \boldsymbol{\mu}_\eta &= E(\mathbf{G}_i^{-1} \times \begin{pmatrix} \eta'_{0i} \\ \eta'_{1i} \\ \eta'_{2i} \\ \delta_i + \mu_\gamma \end{pmatrix}) = E \left[\begin{pmatrix} 1 & -\gamma_i & \gamma_i & 0 \\ 0 & 1 & -1 & 0 \\ 0 & 1 & 1 & 0 \\ 0 & 0 & 0 & 1 \end{pmatrix} \times \begin{pmatrix} \eta'_{0i} \\ \eta'_{1i} \\ \eta'_{2i} \\ \delta_i + \mu_\gamma \end{pmatrix} \right] \\ &\approx \begin{pmatrix} 1 & -\mu_\gamma & \mu_\gamma & 0 \\ 0 & 1 & -1 & 0 \\ 0 & 1 & 1 & 0 \\ 0 & 0 & 0 & 1 \end{pmatrix} \times \begin{pmatrix} \mu_{\eta'_{0i}} \\ \mu_{\eta'_{1i}} \\ \mu_{\eta'_{2i}} \\ \mu_\gamma \end{pmatrix} \end{aligned}$$

under the condition of $\frac{1}{n} \sum_{i=1}^n Cov(\eta_{2i}, \gamma_i) \rightarrow 0$.

⁷It is noted that we have 4 degree-of-freedom when expressing the repeated outcomes of a linear combination of 4 growth factors (Harring et al., 2006). To simplify subsequent calculation, we viewed η_{0i} , η_{1i} , η_{2i} and γ_i (i.e., the growth factors in the original setting) as independent variables. It is also noted that γ_i is intact during the process of reparameterization (?).

Through variance decomposition, we can approximate the variance-covariance matrix of the reparameterized growth factors from the variance-covariance matrix of their original setting via the following equation

$$\begin{aligned}
\Psi_{\eta'} &= \text{Var}(\mathbf{G}_i \times \boldsymbol{\eta}_i) = E(\text{Var}(\mathbf{G}_i \times \boldsymbol{\eta}_i | \gamma_i)) + \text{Var}(E(\mathbf{G}_i \times \boldsymbol{\eta}_i | \gamma_i)) \\
&\approx E(\text{Var}(\mathbf{G}_i \times \boldsymbol{\eta}_i | \gamma_i)) = E(\nabla \mathbf{G}_i \text{Var}(\boldsymbol{\eta}_i) \nabla \mathbf{G}_i^T) \\
&\approx \begin{pmatrix} 1 & \mu_\gamma & 0 & \mu_{\eta_1} \\ 0 & 0.5 & 0.5 & 0 \\ 0 & -0.5 & 0.5 & 0 \\ 0 & 0 & 0 & 1 \end{pmatrix} \Psi_{\eta} \begin{pmatrix} 1 & \mu_\gamma & 0 & \mu_{\eta_1} \\ 0 & 0.5 & 0.5 & 0 \\ 0 & -0.5 & 0.5 & 0 \\ 0 & 0 & 0 & 1 \end{pmatrix}^T \\
&= \nabla \mathbf{G} \Psi_{\eta} \nabla \mathbf{G}^T
\end{aligned} \tag{21}$$

under the condition of $\text{Var}(\gamma_i) \rightarrow 0$ and $\text{Var}(\eta_{1i}) \rightarrow 0$.

Similarly, the variance-covariance matrix of the original parameters can be approximated from the reparameterized setting through the equation

$$\begin{aligned}
\Psi_{\eta} &= \text{Var}(\mathbf{G}_i^{-1} \times \boldsymbol{\eta}'_i) = E(\text{Var}(\mathbf{G}_i^{-1} \times \boldsymbol{\eta}'_i | \gamma_i)) + \text{Var}(E(\mathbf{G}_i^{-1} \times \boldsymbol{\eta}'_i | \gamma_i)) \\
&\approx E(\text{Var}(\mathbf{G}_i^{-1} \times \boldsymbol{\eta}'_i | \gamma_i)) = E(\nabla \mathbf{G}_i^{-1} \text{Var}(\boldsymbol{\eta}'_i) \nabla \mathbf{G}_i^{-1T}) \\
&\approx \begin{pmatrix} 1 & -\mu_\gamma & \mu_\gamma & 0 \\ 0 & 1 & -1 & 0 \\ 0 & 1 & 1 & 0 \\ 0 & 0 & 0 & 1 \end{pmatrix} \Psi_{\eta'} \begin{pmatrix} 1 & -\mu_\gamma & \mu_\gamma & 0 \\ 0 & 1 & -1 & 0 \\ 0 & 1 & 1 & 0 \\ 0 & 0 & 0 & 1 \end{pmatrix}^T \\
&= \nabla \mathbf{G}^{-1} \Psi_{\eta'} \nabla \mathbf{G}^{-1T}.
\end{aligned} \tag{22}$$

under the condition of $\text{Var}(\gamma_i) \rightarrow 0$.

Through the above equations, we noticed that the most critical condition for the approximation to the population-level transformation is $\text{Var}(\gamma_i) \rightarrow 0$. With this condition, the covariances of the knot with other growth factors approach to 0. More importantly, the second item of the expression of variance decomposition in Equations (21) and (22) approaches to 0 given $\text{Var}(\gamma_i) \rightarrow 0$. Though Equation (21) requires $\text{Var}(\eta_{1i}) \rightarrow 0$, whether to satisfy this condition or not does not affect estimation process.

6.3 Expression of each cell of the re-reparameterized mean vector and variance-covariance matrix

$$\begin{aligned}
\mu_{\eta_0} &\approx \mu_{\eta'_0} - \mu_\gamma \mu_{\eta'_1} + \mu_\gamma \mu_{\eta'_2} \\
\mu_{\eta_1} &= \mu_{\eta'_1} - \mu_{\eta'_2} \\
\mu_{\eta_2} &= \mu_{\eta'_2} + \mu_{\eta'_1} \\
\mu_\gamma &= \mu_\gamma \\
\psi_{00} &\approx (\psi'_{11} + \psi'_{22} - 2\psi'_{12})\mu_\gamma^2 + 2(\psi'_{02} - \psi'_{01})\mu_\gamma + \psi'_{00} \\
\psi_{01} &\approx (2\psi'_{12} - \psi'_{11} - \psi'_{22})\mu_\gamma + (\psi'_{01} - \psi'_{02}) \\
\psi_{02} &\approx (\psi'_{22} - \psi'_{11})\mu_\gamma + (\psi'_{01} + \psi'_{02}) \\
\psi_{0\gamma} &\approx (\psi'_{2\gamma} - \psi'_{1\gamma})\mu_\gamma + \psi'_{0\gamma} \\
\psi_{11} &= \psi'_{11} + \psi'_{22} - 2\psi'_{12} \\
\psi_{12} &= \psi'_{11} - \psi'_{22} \\
\psi_{1\gamma} &= \psi'_{1\gamma} - \psi'_{2\gamma} \\
\psi_{22} &= \psi'_{11} + \psi'_{22} + 2\psi'_{12} \\
\psi_{2\gamma} &= \psi'_{1\gamma} + \psi'_{2\gamma} \\
\psi_{\gamma\gamma} &= \psi'_{\gamma\gamma}
\end{aligned}$$

6.4 Details of the transformed matrices and the inverse-transformed matrices between intercept coefficients and path coefficients

$$\begin{aligned}
\boldsymbol{\mu}'_{\eta} &\approx \mathbf{G} \times \boldsymbol{\mu}_{\eta} \iff E(\boldsymbol{\alpha}' + \mathbf{B}' \mathbf{X}_i) \approx \mathbf{G} \times E(\boldsymbol{\alpha} + \mathbf{B} \mathbf{X}_i) \iff \boldsymbol{\alpha}' \approx \mathbf{G} \times \boldsymbol{\alpha} \\
\boldsymbol{\mu}_{\eta} &\approx \mathbf{G}^{-1} \times \boldsymbol{\mu}'_{\eta} \iff E(\boldsymbol{\alpha} + \mathbf{B} \mathbf{X}_i) \approx \mathbf{G}^{-1} \times E(\boldsymbol{\alpha}' + \mathbf{B}' \mathbf{X}_i) \iff \boldsymbol{\alpha} \approx \mathbf{G}^{-1} \times \boldsymbol{\alpha}' \\
\boldsymbol{\Psi}'_{\eta} &\approx \nabla \mathbf{G} \boldsymbol{\Psi}_{\eta} \nabla \mathbf{G}^T \\
&\iff \text{Var}(\boldsymbol{\alpha}' + \mathbf{B}' \mathbf{X}_i + \boldsymbol{\zeta}'_i) \approx \nabla \mathbf{G} \text{Var}(\boldsymbol{\alpha} + \mathbf{B} \mathbf{X}_i + \boldsymbol{\zeta}_i) \nabla \mathbf{G}^T \\
&\iff \text{Var}(\mathbf{B}' \mathbf{X}_i + \boldsymbol{\zeta}'_i) \approx \nabla \mathbf{G} \text{Var}(\mathbf{B} \mathbf{X}_i + \boldsymbol{\zeta}_i) \nabla \mathbf{G}^T \\
&\iff \mathbf{B}' \text{Var}(\mathbf{X}_i) \mathbf{B}'^T + \text{Var}(\boldsymbol{\zeta}'_i) \approx \nabla \mathbf{G} \mathbf{B} \text{Var}(\mathbf{X}_i) \mathbf{B}^T \nabla \mathbf{G}^T + \nabla \mathbf{G} \text{Var}(\boldsymbol{\zeta}_i) \nabla \mathbf{G}^T \\
&\iff \mathbf{B}' \approx \nabla \mathbf{G} \mathbf{B} \\
\boldsymbol{\Psi}_{\eta} &\approx \nabla \mathbf{G}^{-1} \boldsymbol{\Psi}'_{\eta} \nabla \mathbf{G}^{-1T} \\
&\iff \text{Var}(\boldsymbol{\alpha} + \mathbf{B} \mathbf{X}_i + \boldsymbol{\zeta}_i) \approx \nabla \mathbf{G}^{-1} \text{Var}(\boldsymbol{\alpha}' + \mathbf{B}' \mathbf{X}_i + \boldsymbol{\zeta}'_i) \nabla \mathbf{G}^{-1T} \\
&\iff \text{Var}(\mathbf{B} \mathbf{X}_i + \boldsymbol{\zeta}_i) \approx \nabla \mathbf{G}^{-1} \text{Var}(\mathbf{B}' \mathbf{X}_i + \boldsymbol{\zeta}'_i) \nabla \mathbf{G}^{-1T} \\
&\iff \mathbf{B} \text{Var}(\mathbf{X}_i) \mathbf{B}^T + \text{Var}(\boldsymbol{\zeta}_i) \approx \nabla \mathbf{G}^{-1} \mathbf{B}' \text{Var}(\mathbf{X}_i) \mathbf{B}'^T \nabla \mathbf{G}^{-1T} + \nabla \mathbf{G}^{-1} \text{Var}(\boldsymbol{\zeta}'_i) \nabla \mathbf{G}^{-1T} \\
&\iff \mathbf{B} \approx \nabla \mathbf{G}^{-1} \mathbf{B}'
\end{aligned}$$

6.5 Generate Exogenous Variables and Growth Factors Simultaneously

To generate growth factors and exogenous variables simultaneously as a multivariate normal distribution, we need to specify the mean vector and the variance-covariance matrix of the distribution. In our setting, the mean vector can be represented in equation

$$\boldsymbol{\mu} = (\boldsymbol{\alpha} \quad \mathbf{0} \quad \mathbf{0}),$$

where $\boldsymbol{\alpha}$ and $(\mathbf{0} \quad \mathbf{0})$ are the mean vector of the growth factors and that of the TICs, respectively. Moreover, according to the underlying covariance structure of the path analysis model (Hoyle, 2012), the variance-covariance matrix of the distribution is shown in

$$\boldsymbol{\Sigma} = \begin{pmatrix} \mathbf{B}\boldsymbol{\Phi}\mathbf{B} + \boldsymbol{\Psi}_{\eta} & \mathbf{B}\boldsymbol{\Phi} \\ \mathbf{B}\boldsymbol{\Phi} & \boldsymbol{\Phi} \end{pmatrix},$$

where \mathbf{B} is the matrix of path coefficients, $\boldsymbol{\Psi}_{\eta}$ and $\boldsymbol{\Phi}$ are the variance-covariance matrices of the growth factors and the TICs, respectively. Accordingly, we can generate the growth factors and TICs simultaneously, which follows a multivariate normal distribution $N_6(\boldsymbol{\mu}, \boldsymbol{\Sigma})$.